Design and Implementation of the Pillbox Antenna for SASARII

Sifiso Busisa Gambahaya

A dissertation submitted to the Department of Electrical Engineering, University of Cape Town, in partial fulfilment of the requirements for the degree of Master of Science in Engineering.

Cape Town, March 2006

Declaration

I declare that this dissertation is my own, unaided work. It is being submitted to the Department of Electrical Engineering for the degree of Master of Science in Engineering in the University of Cape Town. It has not been submitted before for any degree or examination in any other university.

Signature of Author . . . . . .

Cape Town

March 2006

Abstract

The purpose of this dissertation is to introduce the reader to the radar antenna for SASARII. The dissertation describes the design process, implementation and testing of the radar antenna.

The dissertation starts off by listing all the user requirements that need to be met by the radar antenna for SASARII. The pillbox antenna is introduced as the antenna of choice. The pillbox or cheese antenna as it is also known is then defined and the history of the antenna and the advantages of using the antenna are also given. The design theory necessary for the construction of the antenna is also given.

The dimensions of the feed horn and the dimensions of the aperture to achieve the required beamwidths in the principal E and H-planes are given. The offset-fed pillbox is chosen as the configuration for the antenna. The far-field power patterns of the feed and the antenna are simulated in MATLAB and the directivity of the antenna is calculated.

The antenna tests which include power gain, 3 dB beamwidth, return loss and cross-polarization measurements are discussed. The test results are analyzed and compared to the simulations and theoretical predictions to measure the performance of the antenna.

This dissertation winds up by discussing the conclusions to the research problem and giving suggestions for future improvements to the design.

Acknowledgements

First and foremost I would like to thank my supervisor, Prof. Mike Inggs for his guidance and constant encouragement during the entire research period. Special thanks goes to my family and friends whose constant support was invaluable to the completion of the research.

I would also like to thank Prof. Barry Downing, the RRSG staff, Dr. Richard Lord, Thomas Bennet and all my colleagues in the RRSG for their contributions towards the research.

Contents

List of Figures

List of Tables

List of Symbols

Symbol	—	Definition
A_e	—	Antenna aperture efficiency
B	—	Transmitted RF bandwidth
dBi	—	Decibel over isotropic
D_{az}	—	Azimuth dimension of antenna aperture
D_{el}	—	Vertical dimension of antenna aperture
ϵ	—	Antenna aperture efficiency
ϵ_L	—	Antenna radiation efficiency
$E\left(\theta\right)$	—	Antenna far-field pattern as a function of angle θ
$E_{el}\left(\psi\right)$	—	Antenna elevation far-field pattern
f_o	—	Radar operating frequency
f/D	—	Ratio of focal length to aperture dimension
$F_{az}\left(\psi\right)$	—	Antenna azimuth far-field pattern
G_d	—	Directive gain
G_p	—	Power gain
G_r	—	Receiver gain
G_t	—	Transmitter gain
$G\left(\theta\right)$	—	Gain of antenna as a function of angle θ
$I_{az}(\psi)$	—	Feed power pattern in watts per radian-meter
θ_{az}	—	3 dB azimuth beamwidth
θ_{el}	—	3 dB elevation beamwidth
η	—	Angle off antenna boresight
R	—	Antenna separation
S_{11}	—	Return loss
S_{12}	—	Insertion loss
ψ_f	—	Feed pointing angle
λ	—	Wavelength of carrier signal
ρ_e	—	Slant length of E-plane horn
ρ_h	—	Slant length of H-plane horn
$\rho\left(\psi\right)$	—	Function which defines shape of reflector
τ	—	Reflection coefficient

Nomenclature

Azimuth—Angle in a horizontal plane, relative to a fixed reference, usually north or the longitudinal reference axis of the aircraft or satellite.

Beamwidth—The angular width of a slice through the mainlobe of the radiation pattern of an antenna in the horizontal, vertical or other plane.

3 dB beamwidth—In a plane containing the direction of maximum of a beam, the angle between the two directions in which the radiation intensity is one-half the maximum value of beam.

Boresight—The axis of symmetry of the beam of an antenna.

Co-polarization—That polarization which the antenna is intended to radiate.

Cross-polarization—The polarization orthogonal to a specified reference polarization.

Elevation—Angle in a vertical plane, relative to a fixed reference, usually the latitude reference axis of the aircraft or satellite.

Far-field—Distance where spherical wave front radiated by an antenna approximates the ideal planar phase front of a plane wave.

Synthetic Aperture Radar (SAR)—A signal-processing technique for improving the azimuth resolution beyond the beamwidth of the physical antenna actually used in the radar system. This is done by synthesizing the equivalent of a very long sidelooking array antenna.

X-band—8 to 12.5 GHz frequency band.

AUT	—	Antenna Under Test
CW	—	Continuous Wave mode
EI	—	Edge Illumination
FT	—	Feed Taper
IF	—	Intermediate Frequency
IL	—	Insertion Loss
RL	—	Return Loss
SA	—	Spectrum Analyzer
SMA	—	Type of coaxial cable connector
SPL	—	Spherical spread Loss
TEM	—	Transverse Electromagnetic Wave
UAV	—	Unmanned Aerial Vehicle
VSWR	—	Voltage Standing Wave Ratio

Chapter 1

Introduction

1.1 Background to Project

The SASARII project is an on going initiative to demonstrate the capability of SASAR to implement high quality imagery using (SAR) Synthetic Aperture Radar techniques. The Radar Remote Sensing Group (RRSG) at UCT was commissioned by Kentron, a company that specialises in the design of UAVs (Unmanned Aerial Vehicles) and SunSpace, an engineering company that specialises in the development of small satellites to design, implement and test a high resolution X-band SAR. The SAR system will be deployed on an aircraft and used to take high resolution images of the earth for environmental monitoring purposes irrespective of weather conditions or darkness [21].

This dissertation describes the design, implementation and testing of the radar antenna for SASARII.

1.2 User Requirements

The following requirements were specified for the radar antenna of the SAR system by the system engineer [14] [16] [15].

1. A pillbox antenna with a single mode of propagation is to be designed, implemented and tested to meet specifications.
2. The operating centre frequency is set to $\mathrm{f_{\circ}} = 9.3$ GHz.
3. The antenna operating bandwidth which is determined by the transmitter is $\mathrm{B} = 100\ \mathrm{MHz}$.
4. The antenna 3 dB azimuth beamwidth shall be 3.8° and the elevation beamwidth shall be 25°.
5. The peak power that the antenna system can handle is 3.5 kW.

6. The antenna should be able to operate at a platform height of 3000-8000 m. The platform height is limited by the amount of air at high altitudes. However for reasons of practicality it is unlikely that the aircraft will fly at a height greater than 3000 m, hence we shall limit the platform height to 3000 m.

To review the derivations of the above mentioned user requirements refer to [21] [14] [16] [15].

1.3 Definition of Pillbox Antenna

A pillbox antenna is a linearly polarized cylindrical reflector embedded between two parallel plates. It is usually fed by a waveguide [12] [26]. The pillbox is part of a family of antennas called fan beam antennas which produce a wide beam in one plane and a narrow beam in the other [20].

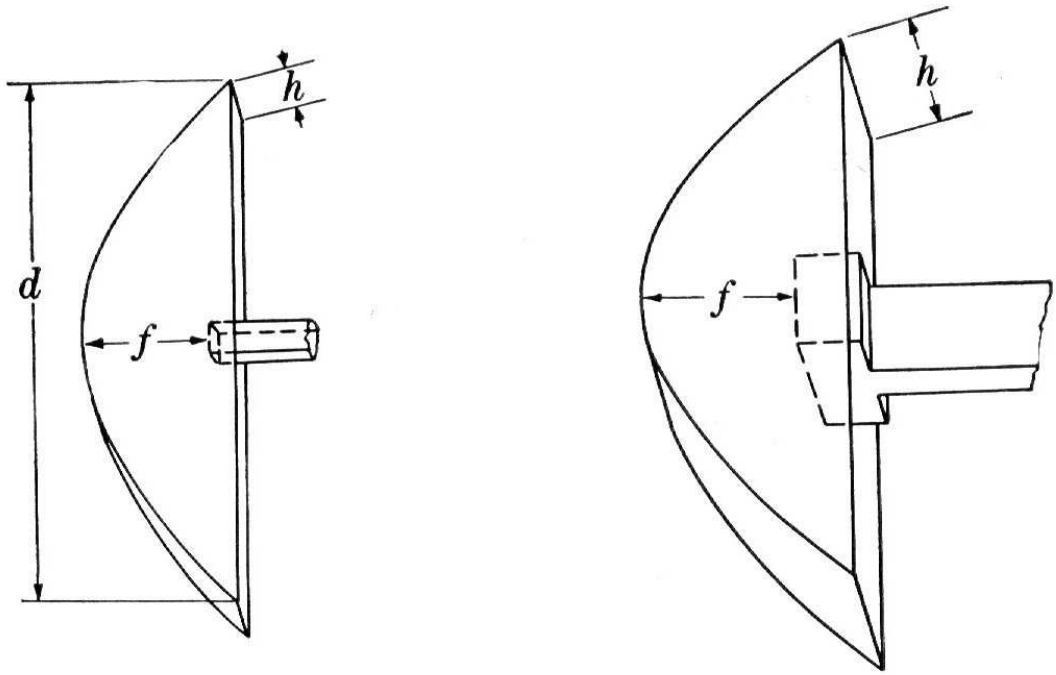

Figure 1.1: Pillbox or Cheese Antenna (from [26])

1.4 History of Pillbox Antenna

The pillbox antenna has existed for at least fifty years and it was used for military radar applications, mostly surveillance during Second World War and just after the Second World War [26]. The British version was called the cheese antenna. The primary difference between the cheese antenna and the pillbox is the separation of the parallel plates and their possible modes of electromagnetic propagation [26] [12].

1.5 Reasons for Choosing the Pillbox Antenna

The reasons for choosing a pillbox antenna over other types of reflector antennas for radar applications are the following [26]:

- It is easy to design and the cost of production is low.
- It is dually-polarized and it is also a wide band antenna.
- It has a high power handling capability.

1.6 Plan of Development

Chapter 2 discusses diffraction theory as well as the aperture field method which is used to predict the far-field patterns in the E and H-planes of the antenna. The relations between directivity and beamwidth of the antenna are also given. We also describe the parallel plates used to confine the electromagnetic energy within the pillbox and the effect of the plate separation on the performance of the antenna.

Chapter 3 discusses the design and construction of the antenna. The dimensions of the feed horn needed to produce the ideal patterns in the E and H-planes of the reflector are calculated. The reflector surface profile is also designed and synthesised. We also discuss the material used and the antenna fabrication process.

Chapter 4 discusses the antenna tests and analysis of the test results.

Chapter 5 concludes the dissertation and gives recommendations for future changes and improvements in design.

Chapter 2

Design Theory of Aperture Antennas

2.1 Diffraction Theory of Aperture Antennas

The radiating aperture of the pillbox antenna is essentially rectangular in shape and the far-field can be derived from Huygens theory [9] [2]. Huygens theory simply states that each point on a propagating wavefront at the aperture can be represented by an ideal secondary point source of electric field radiating spherical waves [9]. In the far-field region, the summation or superposition of the secondary waves gives us an angular dependant diffraction pattern which is equivalent to the far-field pattern of the antenna.

2.2 Aperture Field Method

By using geometrical optics [9] and the diffraction theory of antennas we can predict the far-field of an antenna. There is a Fourier Transform relationship between the far-field and the aperture field which is analogous to the relationship between Fourier spectra and waveforms (even though waveforms are one-dimensional). The far-field can be predicted by taking the Fourier Transform of the tangential component of the E-field. This one dimensional treatment is adequate for discussing the pillbox antenna since its directivity can be separable into a product of directivities of one-dimensional apertures made up of the length and width of the aperture [3]. Once the aperture fields are have been calculated, we use equation 2.1 to predict the far-field pattern of the antenna in the E and H-planes [9][10][6]:

$$\mathrm{E}(\theta) \quad = \quad \int_{-\mathrm{x}/2}^{\mathrm{x}/2} \mathrm{f}(\mathrm{x})\, e^{\mathrm{jkx}\sin\theta} \mathrm{dx} \tag{2.1}$$

Where
$\mathrm{f}(\mathrm{x})$ is the aperture field distribution function across the aperture, 'x' is the length of the aperture and 'k' is the wavenumber.

2.3 Directivity and Gain

The gain of an antenna is described by its ability to concentrate energy in a narrow angular region. There are two different but related definitions of antenna gain, being the $directive\ gain$ and the $power\ gain$. The directive gain is usually referred to as the $directivity$ and the power gain simply as $gain$. Strictly speaking the $directive\ gain$ is the radiation intensity in any direction θ relative to the average intensity of an isotropic radiator [23]. In the far-field region R, the directivity of an antenna is given by the following expression [27]:

$$\begin{aligned} \mathrm{G_d} &= \frac{\text{maximum radiation intensity}}{\text{average radiation intensity}} \\ &= \frac{\text{maximum radiation pattern density}}{\text{total radiated power}/4\pi} \end{aligned} \tag{2.2}$$

The above expression also applies to the definition of directivity for aperture antennas. This can also be expressed in terms of the maximum radiated-power density (in watts per square meter) at a far-field distance R relative to the average density of an isotropic radiator at that same distance. This definition tells us how much stronger the maximum power density is than it would be if it were radiated isotropically. Dissipation of power is not accounted for in this definition given by [27]:

$$\begin{aligned} \mathrm{G_d} &= \frac{\text{maximum power density}}{\text{total power radiated}/4\pi\mathrm{R}^2} \\ &= \frac{\mathrm{P_{max}}}{\mathrm{P_t}/4\pi\mathrm{R}^2}\ \left[\mathrm{W/m^2}\right] \end{aligned} \tag{2.3}$$

The power gain or simply the gain $\mathrm{G_p}$ of the antenna referred to an isotropic source is the ratio of its maximum radiation intensity to the radiation intensity of a lossless isotropic source with the same power input [5].

$$\begin{aligned} \mathrm{G_p} &= \frac{\text{maximum power density}}{\text{total power accepted}/4\pi\mathrm{R}^2} \\ &= \frac{\mathrm{p_{max}}}{\mathrm{P_\circ}/4\pi\mathrm{R}^2}\left[\mathrm{W/m^2}\right] \end{aligned} \tag{2.4}$$

Where $\mathrm{P_\circ}$ is the power accepted by the antenna at its input terminals.

The power gain of an antenna is related to its directivity as follows [24]:

$$\mathrm{G_p} \;=\; \epsilon_\mathrm{L}\mathrm{G_d}\;\left[\mathrm{W/m^2}\right] \tag{2.5}$$

The radiation efficiency of the antenna is given by [24]:

$$\begin{aligned}\epsilon_\mathrm{L} &= \frac{\mathrm{P_{rad}}}{\mathrm{P_{in}}} \\ &= \frac{\mathrm{P_{in}} - \mathrm{P_{loss}}}{\mathrm{P_{in}}}\end{aligned} \tag{2.6}$$

Where
$\mathrm{P_{in}}$ is the power supplied to the input of the antenna,
$\mathrm{P_{rad}}$ is the power radiated by the antenna,
$\mathrm{P_{loss}}$ is the power lost in the antenna due to resistive losses [24].

The above mentioned definitions are consistent with the **"IEEE Standard Parameter Definitions of Terms for Antennas"** (IEEE STD-145) which defines the above mentioned parameters as follows:

Directive Gain–In a given direction, 4 times the ratio of the radiation intensity in that direction to the total power radiated by the antenna. Directivity is defined as–the value of the directive gain in the direction of its maximum value [1].

Directivity–The value of the directive gain in the direction of its maximum value [1].

Power Gain–In a given direction, 4 times the ratio of the radiation intensity in that direction to the net power accepted by the antenna from the connected transmitter [1].

2.3.1 Directivity-Beamwidth Relations

An approximate relationship between directivity and antenna beamwidth is given by [2]:

$$\mathrm{G_d} \;\approx\; \frac{4\pi}{\theta_\mathrm{az} \cdot \theta_\mathrm{el}} \tag{2.7}$$

Where
θ_az and θ_el are the 3 dB beamwidths (in radians) in the horizontal and vertical planes respectively.

2.3.2 Effective Aperture

The directivity of an aperture antenna may also be calculated from the physical dimensions of the antenna. The aperture of an antenna is defined as its physical area projected on a

plane perpendicular to the main beam direction. Most aperture antennas have a tapered illumination and are not uniformly illuminated (maximum in the centre of the aperture and less at the edges) so as to reduce the sidelobes of the pattern. The directivity may be determined from the aperture dimensions as [27]:

$$\mathrm{G_d} \;=\; \frac{4\pi \mathrm{A}_e}{\lambda^2} \tag{2.8}$$

Where
$\mathrm{A_e}$ is the effective aperture, less then the physical area A by a factor ϵ which is called the aperture efficiency.

$$\mathrm{A}_e \;=\; \epsilon \mathrm{A} \;\left[\mathrm{m}^2\right] \tag{2.9}$$

2.4 Parallel-Plate Systems

The side plates of a pillbox antenna act as a parallel plate waveguide. Their main purpose is to guide the radiation from the primary feed to the parabolic reflector [20]. The separation of the plates also determines the mode of propagation between the plates [20]. The separation of the plates determines the beamwidth of the antenna in the plane of separation. Parallel-plate systems may be classed into two groups [26]:

- If $\mathrm{h} < \lambda/2$ propagation between the plates is limited to the principal or TEM mode.
- Parallel-plate systems with spacing $\mathrm{h} > \lambda$ which support additional modes. These are called cheese antennas.

Where
h is the separation of the plates.

2.5 Power Radiation Patterns

The shape of the aperture field distribution of the antenna determines the gain pattern of that antenna. For an antenna with a sinc or $\sin(\mathrm{x}/\mathrm{x})$ pattern the normalized power radiation pattern in the azimuth direction θ for a uniform aperture illumination is given by the following [19] :

$$\mid \mathrm{E}(\theta) \mid^2 \;=\; \left[\frac{\sin\left[\frac{\pi \mathrm{d}}{\lambda}\right]\sin(\eta)}{\frac{\pi \mathrm{d}}{\lambda}\sin(\eta)}\right]^2 \tag{2.10}$$

where
η is the angle off boresight and d is the aperture dimension. Therefore it follows that the normalized E-field squared gives the gain, $\mathrm{G}(\theta)$ of an antenna [22].

A double-sinc pattern results for a co-sinusoidal aperture distribution and the normalized power radiation pattern is given by the following expression in [2] [12]:

$$|\,\mathrm{E}(\theta)\,|^2 \;=\; \left[\pi^2 \cos(\eta)\,\frac{\cos\left[\frac{\pi \mathrm{d}}{\lambda}\sin(\eta)\right]}{\pi^2 - 4\left[\frac{\pi \mathrm{d}}{\lambda}\sin(\eta)\right]^2}\right]^2 \tag{2.11}$$

Hence we can say the modulus squared of the normalised angular spectrum gives the gain pattern of an antenna.

2.6 Conclusion

This chapter has discussed the relevant background theory required to design a pillbox antenna. Diffraction theory and the aperture field method have been discussed. It has been given that one can determine the radiation pattern of an aperture antenna by taking the Fourier transform of its aperture fields. The effect of separation of the parallel plates on the mode of propagation within the antenna has been discussed. The important relationships between beamwidth and directivity have been given. The next chapters will build on the basic theory developed in this chapter. The aperture field method will be used to predict the far-field radiation patterns, hence the 3 dB beamwidths of the antenna in the E and H-planes through MATLAB simulations. The directivity of the antenna will also be calculated from its radiation pattern. This is discussed in Chapter 3.

Chapter 3

Design and Construction of Antenna

3.1 Offset-fed Parabolic Reflector Design

Offset prime-focus-reflectors are desirable because of the ability to offset the feed enough so that it is not in the way of the aperture to cause aperture blockage which consequently raises the sidelobe levels. However, offset-fed reflectors with a linearly polarized feed suffer from higher cross-polarization than axisymmetric reflectors [28]. Here the major design emphasis is on the choice of offset angle or feed pointing angle ψ_{f} to reducing sidelobe levels and also reduce cross polarization without a sacrifice in gain [28].

Offset reflector antennas inherently produce off-axis cross-polarization in the principal plane normal to the offset plane. The cross-polarization is a result of the asymmetric mapping of the otherwise symmetrical pattern into the aperture antenna [25]. We wish to keep the cross-polarization levels to at least 30 dB below the peak of the co-polar pattern for satisfactory performance of the antenna [25] [20].

3.1.1 The Geometry

The geometry of the offset fed configuration is shown in Figure 3.1. The primary parameters that we can control are the degree of offset by varying the distance of offset "h", (see Figure 3.1) and the aiming of the feed antenna $(\text{the angle } \psi)$. In our design we consider the case of the more than fully offset feed, $\mathrm{h} > 0$ to provide a blockage-free region for the structures in the focal region. In practice in order to keep spill-over losses reasonable the feed is aimed within the range [26] [28] :

$$40^{\circ} \leq \quad \psi_{\mathrm{f}} \leq \quad 60^{\circ} \tag{3.1}$$

The definitions of the symbols used in Figure 3.1 are given below where

D	=	Diameter of the projected aperture of the parabolic cylinder
h	=	Offset distance=distance from the axis of the symmetry to the lower reflector edge.
$\mathrm{D_p}$	=	Diameter of the projected circular aperture of the parent paraboloid.
f	=	f =Focal length.(shown as F in figure 3.1)
$\mathrm{f/D_p}$	=	f/D' of parent reflector.
ψ_f	=	Angle of antenna pattern peak relative to reflector axis of symmetry (ies)
ψ_c	=	Value of ψ_f when the feed is aimed at the aperture centre.
ψ_E	=	Value of $\psi_\mathrm{f}$when the feed yields an equal edge illumination .
ψ_B	=	Value of ψ_f which bisects the reflector subtended angle.
ψ_p	=	Angle from the lower edge of the reflector to the angle $\psi_\mathrm{p} = \psi_\mathrm{S} + \psi_\mathrm{L}$.
FT	=	Feed edge taper; $\mathrm{FT} \geq 0$.
EI	=	Edge illumination; $\mathrm{EI} = -(\mathrm{FT} + \mathrm{SPL})$; SPL is the spherical spread loss .

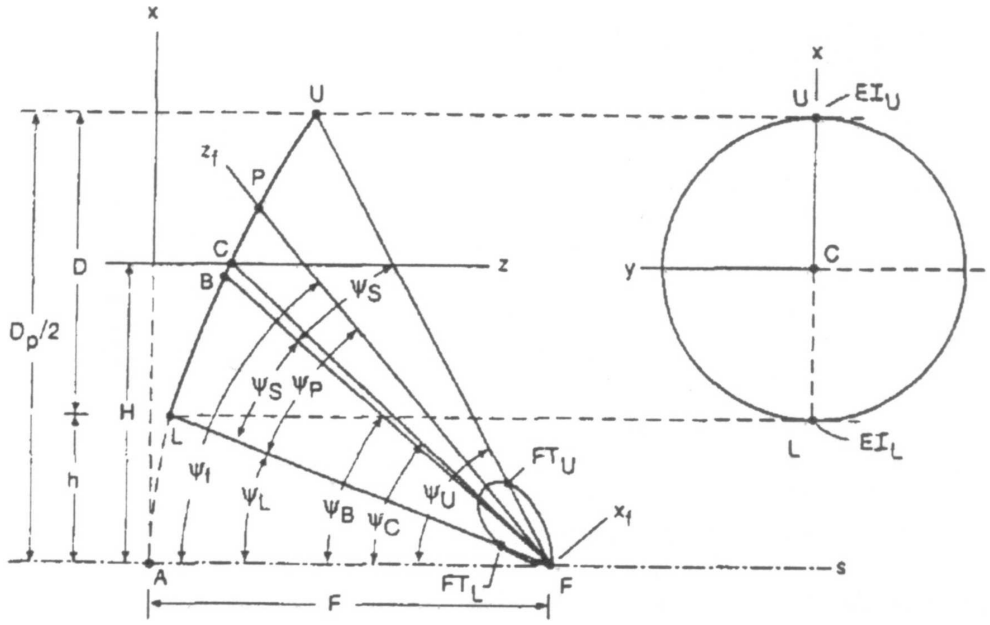

Figure 3.1: Offset Parabolic Reflector Geometry (from [28])

The spherical spread loss of the antenna is given by [28] :

$$\mathrm{SPL}\,(\psi) \;=\; -20\log\left[\cos^2\frac{\psi}{2}\right] \tag{3.2}$$

Quoting "W. Stutzman and Terada", several numerical simulations using the physical optics computer code $GRASP-7$ on reflector antennas yielded the following results [28] :

- Several numerical simulations showed that the orientation of the feed strongly influences cross-polarization. In particular small feed pointing angles lead to high spillover which would raise the sidelobe and cross-polarization levels for high gains.

- Large $\mathrm{f/D_p}$ values which lead to reduced feed pointing angles ψ_f cause degradation in sidelobe levels even though the cross-polarization level improves. Based on the above observations, we can thus try to optimize the feed pointing or offset angle to yield the lowest sidelobes and cross-polarization levels with the smallest penalties in gain. A feed pointing angle of $\psi_\mathrm{f} = \psi_\mathrm{E}$ achieves this specification and it also turns out that this operating point produces a balanced aperture illumination, that is the edge illumination levels (in the plane of offset) in the aperture are equal.

The diameter of the parent parabola was fixed at $\mathrm{D_p} = 126$ cm and curvature of the reflector was $\mathrm{f/D_p} = 0.3$ to achieve a good compromise between sidelobe levels and cross-polarization.

3.1.2 Reflector Aperture Dimensions

We calculated the angles ψ_L and ψ_U which are the angles subtended by the lower and upper edges of the reflector respectively using equation 3.2 [22] :

$$\rho\left(\psi\right) \;=\; 2\mathrm{f}\tan\left(\frac{\psi}{2}\right) \tag{3.3}$$

- The angle subtended by the upper edge of the reflector is calculated as follows:

$$\begin{aligned}\psi_\mathrm{U} \;&=\; 2\cdot\arctan\left(\frac{64}{2\times 38}\right)\\ &\approx\; 80^\circ\end{aligned} \tag{3.4}$$

- The angle subtended by the lower edge of the reflector is calculated as follows:

$$\begin{aligned}\psi_\mathrm{L} \;&=\; 2\cdot\arctan\left(\frac{7}{2\times 38}\right)\\ &\approx\; 11^\circ\end{aligned} \tag{3.5}$$

where

ρ is the perpendicular distance from the parent reflector centre to the upper edge.

The feed pointing angle $\psi_\mathrm{f} \simeq \psi_\mathrm{E}$ is calculated by a graphical method given in APPENDIX C.2 to be $\psi_\mathrm{E} = 49^\circ$[1]. When the feed is pointed at $\psi_\mathrm{f} \simeq \psi_\mathrm{E}$, a feed taper imbalance is

[1]The feed angle in the MATLAB simulation was $\psi_\mathrm{B} = 45^\circ$, when the antenna was constructed the feed was infact pointed at 45° and not $\psi_\mathrm{E} = 49^\circ$.

created which causes an equal edge illumination at the reflector. A simple MATHCAD calculation gave the length of the feed horn in the offset plane to achieve an equal edge illumination of approximately -10 dB at the edges. The length of the horn was calculated to be 6.5 cm (see APPENDIX A.2). It was only later discovered that there was an error in the initial calculation of the horn azimuth dimension, it should have been 6 cm instead.

- The additional taper due to the space loss in ψ_{L} is small and can be neglected. The SL at ψ_{U} is calculated as follows:

$$\begin{aligned} \mathrm{SPL_U} &= -20\log\left[\cos^2\left(\frac{80}{2}\right)\right] \\ &= 4.5 \ [\mathrm{dB}] \end{aligned} \tag{3.6}$$

The space loss will introduce an additional 4.5 dB taper in the secondary aperture field distribution at the upper edge of the reflector.

- The length $\mathrm{D_{az}}$of the aperture required to produce an edge illumination of -10 dB at the reflector edges is calculated by the following equation:

$$\begin{aligned} \mathrm{D_{az}} &= (1.05\mathrm{A_{edge}} + 55.95)\,\frac{\lambda}{\theta_{\mathrm{az}}} \\ &= ((1.05^\circ \times 10) + 55.95)\,\frac{3.2}{3.8} \\ &= 56 \ [\mathrm{cm}] \end{aligned} \tag{3.7}$$

- The width of the aperture for a uniform illumination in the elevation plane is calculated by the following equation:

$$\begin{aligned} \mathrm{D_{el}} &= \frac{57\lambda}{\theta_{\mathrm{el}}} \\ &= \frac{57 \times 3.2}{25} \\ &= 7 \ [\mathrm{cm}] \end{aligned} \tag{3.8}$$

- The offset distance was set to $\mathrm{h} = \mathrm{D}/8$ so that '$\mathrm{h} = 7\,\mathrm{cm}$'.

3.1.3 Aperture Field Method

We used the aperture field method to determine the offset reflector pattern in the azimuth plane at $\psi_{\mathrm{f}} = 45^{\circ}$. We evaluated the equivalent Huygens sources at the aperture and integrated these sources to obtain the reflector far-field pattern [12]. This section shows the steps taken to predict the reflector far-field.

The equation of the parabolic cylinder in polar coordinates is given as [9]:

$$\begin{aligned} \rho(\psi) &= \frac{\mathrm{f}}{\cos^2(\psi/2)} \\ &= \frac{2\mathrm{f}}{1+\cos\psi} \end{aligned} \tag{3.9}$$

The primary and secondary power flows are equal and given as [9]:

$$\mathrm{P(y)} = \mathrm{I}(\psi)\,\mathrm{dy} \tag{3.10}$$

Where

$\mathrm{I_{az}}(\psi)$ is the feed far-field power pattern of the horn in units of watts per radian-meter.

$\mathrm{P(y)}$ is the secondary power flow in units of watts per radian-meter.

The feed radiation pattern in the H-plane is modelled by the following Fourier Transform expression at the feed pointing angle $\psi_{\mathrm{f}} = 45^{\circ}$ [12]:

$$\mathrm{E_{az}}(\psi - \psi_{\mathrm{offset}}) = \int_{-\mathrm{a_1}/2}^{\mathrm{a_1}/2} \mathrm{E_0}\cos\left(\frac{\pi}{a}\right) e^{j\frac{2\pi}{\lambda}\mathrm{x}\sin(\psi-\psi_{\mathrm{offset}})}\mathrm{dx} \tag{3.11}$$

The azimuthal power pattern of the horn is given by:

$$\mathrm{I_{az}}(\psi) = \mathrm{I_{az}^2}(\psi - \psi_{\mathrm{offset}}) \tag{3.12}$$

The equation relating the primary and secondary power distributions is given by the following expression [9]:

$$\begin{aligned} \mathrm{P}(y) &= \frac{\mathrm{I}(\psi)}{\rho(\psi)} \\ &= \frac{\mathrm{I_{az}}(\psi)\cos^2(\psi/2)}{\mathrm{f}} \end{aligned} \tag{3.13}$$

The aperture field of the reflector is given by the following expression [9]:

$$\mathrm{f_{az}\,(y)} \quad = \quad \mathrm{P\,[(y)]^{1/2}} \tag{3.14}$$

The far-field pattern of the reflector is then given by the following Fourier Transform expression [9]:

$$\mathrm{F_{az}\,(\psi)} \quad = \quad \int_{-\mathrm{D_{az}}/2}^{\mathrm{D_{az}}/2} \mathrm{f_{az}\,(y)}\, e^{j\frac{2\pi}{\lambda} y \sin\psi} \mathrm{dy} \tag{3.15}$$

Where
h = Offset distance = distance from the axis of symmetry(ies) to the lower reflector edge
$\mathrm{D_{az/2}}$ is half the span of the parent parabola.

3.1.4 Predicted Azimuth Pattern (H-plane)

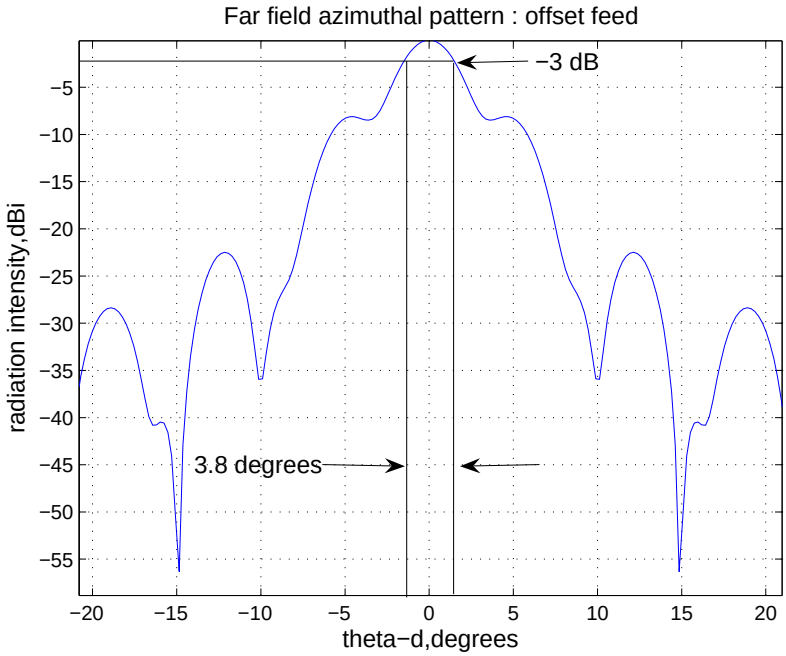

Figure 3.2: Predicted Azimuth Power Pattern (H-plane , dB w.r.t peak gain)

Figure 3.2 shows the predicted H-plane pattern of the pillbox antenna which was simulated in MATLAB for an azimuth aperture dimension of 56 cm. The 3 dB beamwidth was found to be 3.8° which was the same as the theoretically predicted value from equation. The first sidelobe levels where found to be -23 dB. The predicted pattern does however seem to possess some unexpected features. There are hidden sidelobes at about $\pm 5^\circ$below

the peak of the main beam. This usually corresponds to a quadratic phase error across the aperture

3.1.5 Predicted Elevation Pattern (E-plane)

Assuming the $tangent\ plane\ approximation\ of\ physical\ optics$ [6], we can predict the elevation pattern by the following expression:

$$\mathrm{E_{el}}\left(\psi\right) \quad = \quad \int_{-\mathrm{D_{el}}/2}^{\mathrm{D_{el}}/2} \mathrm{E_{\circ}} e^{j\frac{2\pi}{\lambda} y \sin\psi} \mathrm{dy} \tag{3.16}$$

Where
$\mathrm{D_{el}}/2 \leq h \leq -\mathrm{D_{el}}/2$ is the height of the pillbox aperture.
The power radiation pattern in the vertical plane is given by [12] :

$$\mathrm{P_{el}}\left(\theta\right) \quad = \quad \mathrm{E_{el}^{2}}\left(\theta\right) \tag{3.17}$$

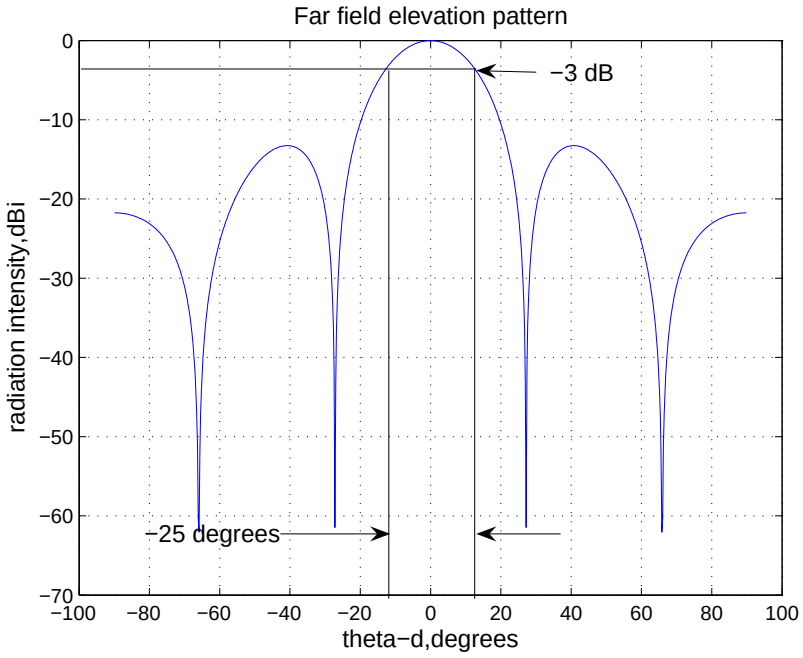

Figure 3.3: Predicted Elevation Power Pattern (E-plane, dB w.r.t peak gain)

3.2 Directivity of the Pillbox Antenna

The directivity of the pillbox antenna was approximated from the following expression [2] [24] [23]:

$$
\begin{aligned}
\mathrm{G_D} &\approx \frac{1}{\mathrm{k}} \cdot \frac{4\pi}{\theta_{\mathrm{az}} \cdot \theta_{\mathrm{ele}}} \\
&= \frac{4\pi}{0.44 \times 0.066 \times 1.12} \\
&= 25.6 \ [\mathrm{dBi}]
\end{aligned} \tag{3.18}
$$

Where
θ_{az} and θ_{el} are the principal azimuth and elevation planes respectively.
k is the beam broadening factor relative to a uniform distribution, which is also the loss in directivity.

3.3 Design of Feed Horn

3.3.1 Pyramidal Horn Design

The most widely used horn is the one which is flared in both directions as shown in the figure. It is widely referred to as a pyramidal horn and its radiation characteristics are essentially a combination of the E and H-plane sectoral horns [2]. For a $\mathrm{TE}_{1,0}$ mode horn, the electric field distribution consists of a uniform amplitude distribution across the 'a' dimension and a half cosine tapered amplitude distribution across the 'b' dimension. The phase variation is parabolic across both dimensions [6].

The electric field across the 'a' dimension which is representative of the horn aperture field in azimuth is given by the expression

$$
\mathrm{E_a} = \mathrm{E_o} \cos\left(\frac{\pi x}{\mathrm{a}}\right) \tag{3.19}
$$

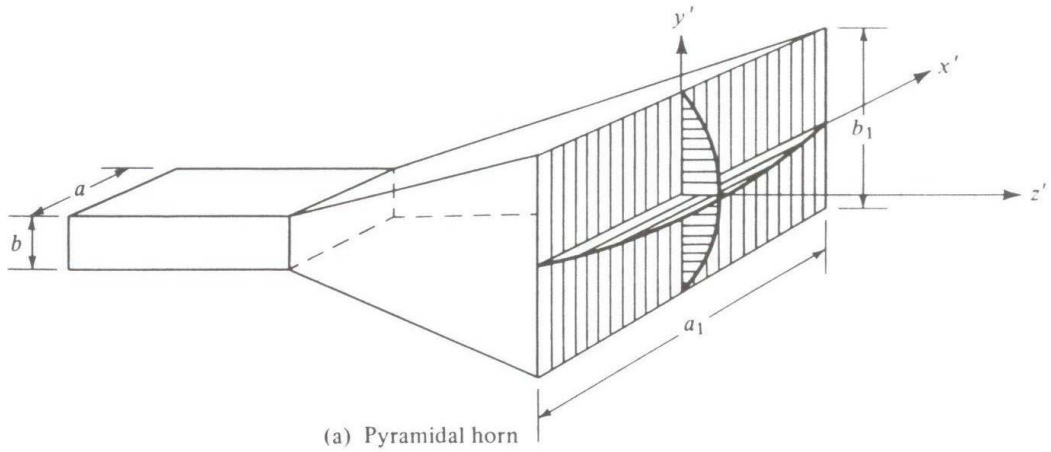

Figure 3.4: Pyramidal Horn: (from [2]).

A pyramidal horn can only be constructed for dimensions that satisfy the following equation [2] [17]:

$$(\mathrm{a_1}-\mathrm{a})^2\left[\left(\frac{\rho_\mathrm{h}}{\mathrm{a_1}}\right)^2-\frac{1}{4}\right] \;=\; (\mathrm{b_1}-\mathrm{b})^2\left[\left(\frac{\rho_e}{\mathrm{b_1}}\right)^2-\frac{1}{4}\right] \tag{3.20}$$

where $p_e = p_h$.

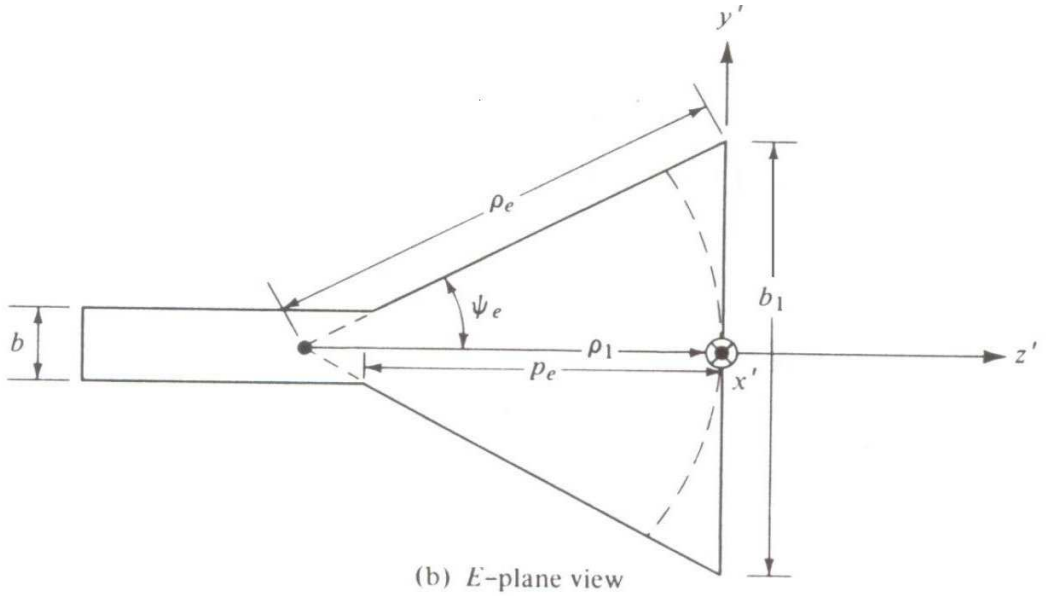

Figure 3.5: E-plane View (from [2]).

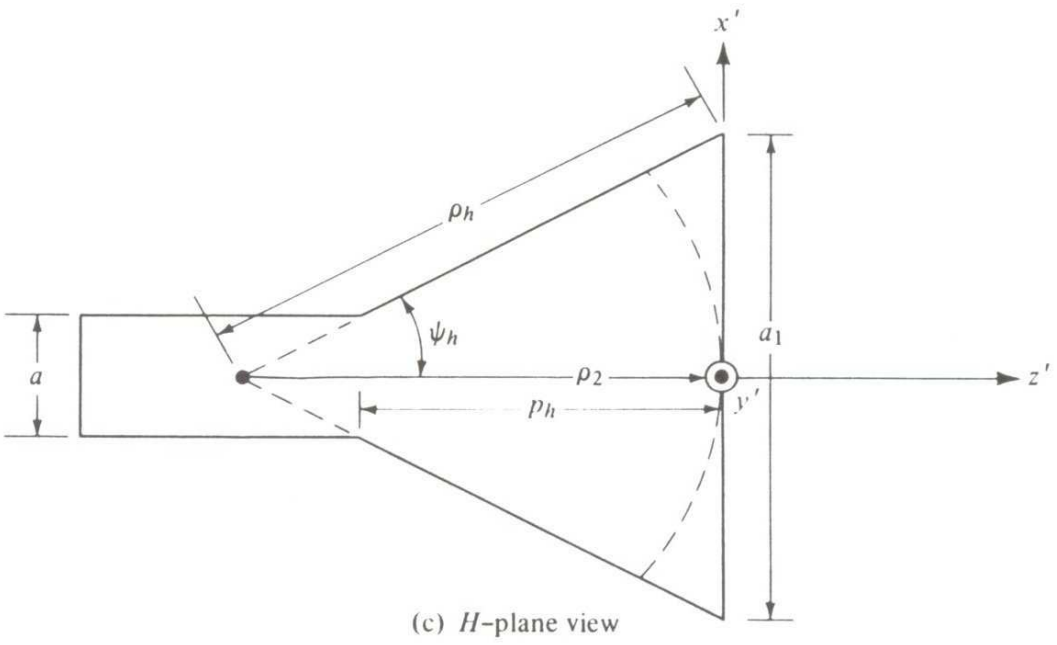

Figure 3.6: H-plane View (from [2]).

The longer the length ρ of the horn antenna, the smoother the transition from 'a' and 'b' to a_1 and b_1 respectively. Practical limitations usually limit the minimum ρ, below which the performance of the horn is degraded appreciably [2]. This value is typically 20° of flare angle [9]. A horn will not support free propagation of a particular mode until roughly the transverse dimensions of the horn exceed those of a waveguide which would support the given mode. Thus unless the flare angle is too large all modes of propagation will be attenuated (except the dominant one of course) to a negligible amplitude in the throat region before free propagation in the horn is possible [26] [7].

3.3.2 Calculation of Horn Dimensions

Pyramidal Horn Dimensions

From Section 3.1.2 we were able to determine the horn dimension a_1 in MATHCAD that gives a -10 dB edge illumination in the azimuth plane. We evaluated this to be $\mathrm{a}_1 = 6.5$ cm. The $\mathrm{TE}_{1,0}$ waveguide dimension a $= 2.286$ cm. In the elevation plane the horn dimension b_1 is determined by the separation of the plates, therefore $\mathrm{b}_1 = 7$ cm. The $\mathrm{TE}_{1,0}$ waveguide dimension $\mathrm{b} = 1.016$ cm.

- We chose a flare angle of 20° in the E-plane and using simple trigonometry, the slant length in the E-plane is calculated as follows:

$$\rho_\mathrm{e} = \frac{3.5}{\sin 20}$$

$$\rho_{\mathrm{e}} \;=\; 10.23\ [\mathrm{cm}] \tag{3.21}$$

- By making use of equation 3.13 and making ρ_{h} the subject of the formula, the slant length in the H-plane is calculated as follows:

$$\begin{aligned}
(\mathrm{a}_1-\mathrm{a})^2\left[\left(\frac{\rho_{\mathrm{h}}}{\mathrm{a}_1}\right)^2-\frac{1}{4}\right] &= (\mathrm{b}_1-\mathrm{b})^2\left[\left(\frac{\rho_e}{\mathrm{b}_1}\right)^2-\frac{1}{4}\right] \\
(6.5-2.286)^2\left[\left(\frac{\rho_{\mathrm{h}}}{6.5}\right)^2-\frac{1}{4}\right] &= (7-1.016)^2\left[\left(\frac{10.23}{7}\right)^2-\frac{1}{4}\right] \\
\left(\frac{\rho_{\mathrm{h}}}{6.5}\right)^2 &\approx 4.055 \\
\rho_{\mathrm{h}} = \;& 13.09\ [\mathrm{cm}]
\end{aligned} \tag{3.22}$$

- From simple trigonometry, $\rho_{\mathrm{h}} = 13.09$ cm corresponds to an H-plane flare angle calculated as:

$$\begin{aligned}
\psi_{\mathrm{h}} &= \arcsin\left(\frac{3.25}{13.09}\right) \\
\psi_{\mathrm{h}} &= 14.5^{\circ}
\end{aligned} \tag{3.23}$$

3.4 Predicted E and H-plane Horn Patterns

3.4.1 H-plane Pattern

The far-field pattern of the feed in the H-plane is given by the following Fourier Transform expression [12] :

$$\mathrm{E}_{\mathrm{az}}\left(\psi-\psi_{\mathrm{offset}}\right) \;=\; \int_{-\mathrm{a}_1/2}^{\mathrm{a}_1/2}\mathrm{E}_{\circ}\cos\left(\frac{\pi \mathrm{x}}{\mathrm{a}_1}\right)e^{j\frac{2\pi}{\lambda}x\sin(\psi-\psi_{\mathrm{offset}})}\mathrm{dx} \tag{3.24}$$

The feed power pattern is given by [12]:

$$\begin{aligned}
\mathrm{P}_{\mathrm{az}}\left(\psi-\psi_{\mathrm{offset}}\right) &= \mathrm{I}_{\mathrm{az}}\left(\psi\right) \\
&= \mathrm{E}^2_{\mathrm{az}}\left(\psi-\psi_{\mathrm{offset}}\right)
\end{aligned} \tag{3.25}$$

Figure 3.7 shows the MATLAB prediction of the H-plane offset feed pattern. The angle of offset is $45^{\circ}$and the 3 dB beamwidth is 37°. This is in agreement with the theoretical prediction which can be calculated from Equation 3.6.

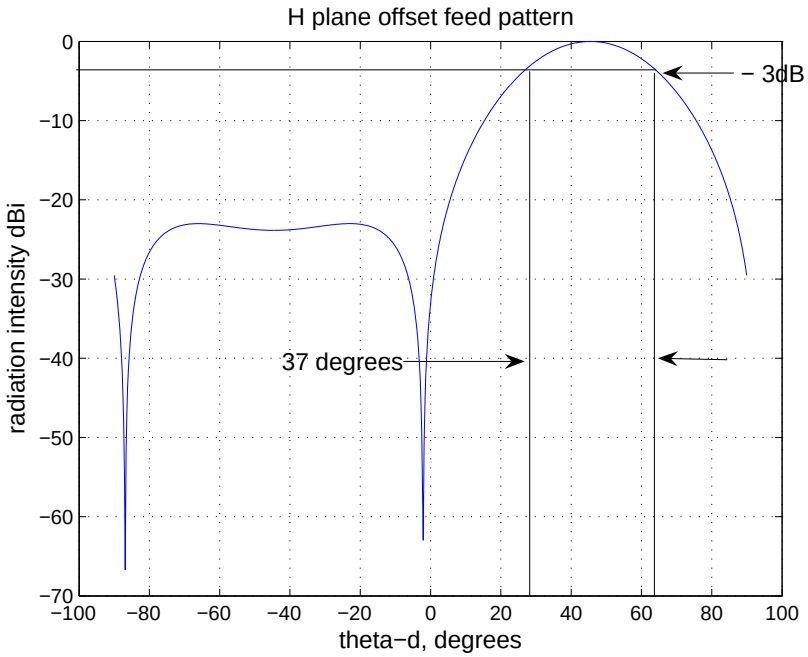

Figure 3.7: Predicted Offset Feed Pattern

3.4.2 E-plane Pattern

The magnitude of the aperture field along the vertical dimension $\mathrm{b_1}$ is simply $\mathrm{E_\circ}$ due to the uniform E-field distribution. The far-field pattern is given by the following Fourier Transform expression:

$$\mathrm{E_{el}}\left(\psi\right) \quad = \quad \int_{-\mathrm{b_1}/2}^{\mathrm{b_1}/2} e^{\mathrm{j}\frac{2\pi}{\lambda}\mathrm{y}\sin\psi}\mathrm{dy} \tag{3.26}$$

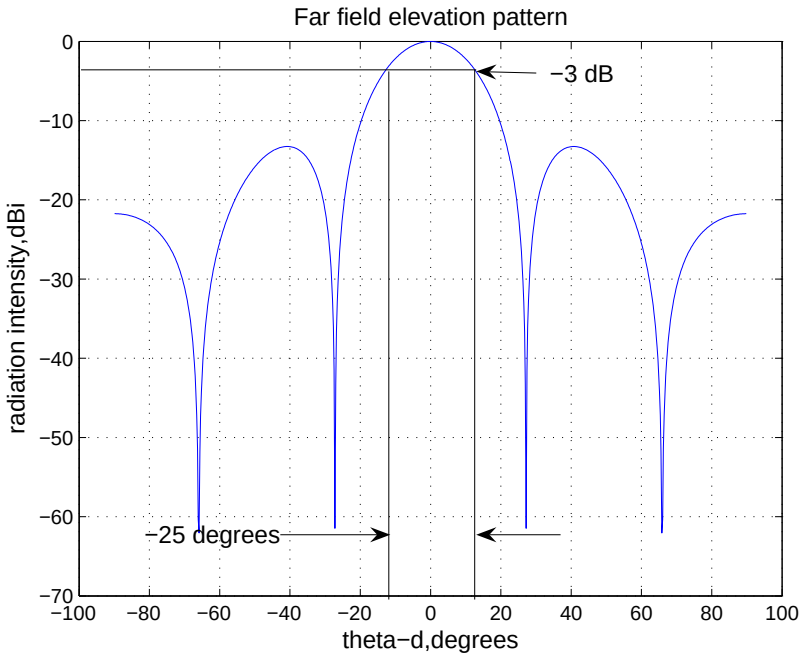

Figure 3.8: Predicted E-plane Feed Pattern (dB w.r.t peak gain)

3.5 Antenna Construction

Once the dimensions of the feed and the pillbox had been determined, CAD drawings were made from which the surface profiles were laser cut to the right dimensions and the structures sent to the Mechanical Engineering Workshop at UCT for fabrication and assembly. The feed horn was made out of brass of 1 mm thickness and the parallel plates as well as the cylindrical reflector were made out of 2mm thick aluminium.

The horn sides were then soldered together to form the horn and the parallel plates were welded (with difficulty) onto the shaped cylindrical reflector to form the pillbox cavity. PVC dielectric posts were used to support the parallel plates. All the welding was done at the Mechanical Engineering Workshop at UCT.

Two slots were cut out of the bottom and the top plate along the feed axis where the feed was embedded between the two parallel plates at a pointing angle of 45° along the feed axis. The feed was placed on the focal point of the reflector and made movable back and forth so as to locate the phase centre.

The key aspects in the manufacturing of the antenna prototype are listed below:

- The plates had to be flat with no bending as this might excite modes other than TEM.
- The feed positioning is important and in this regard it was designed so that it was embedded between the parallel plates and made movable back and forth so as to locate the phase centre. Plastic screws were used to fasten the feed in place.

- We avoided vertical walls on either side of the pillbox as these might cause internal reflections and affect performance as well as possibly short out the E field and cause propagation of higher modes. Instead we used PVC dielectric posts to support the parallel plates and maintain rigidity.

- Any gaps between the plates and the reflector were avoided as this would cause radiation leakage and this might affect the far-field pattern and gain measurements. However we assumed that tiny gaps created by bending the reflector should not affect our readings significantly.

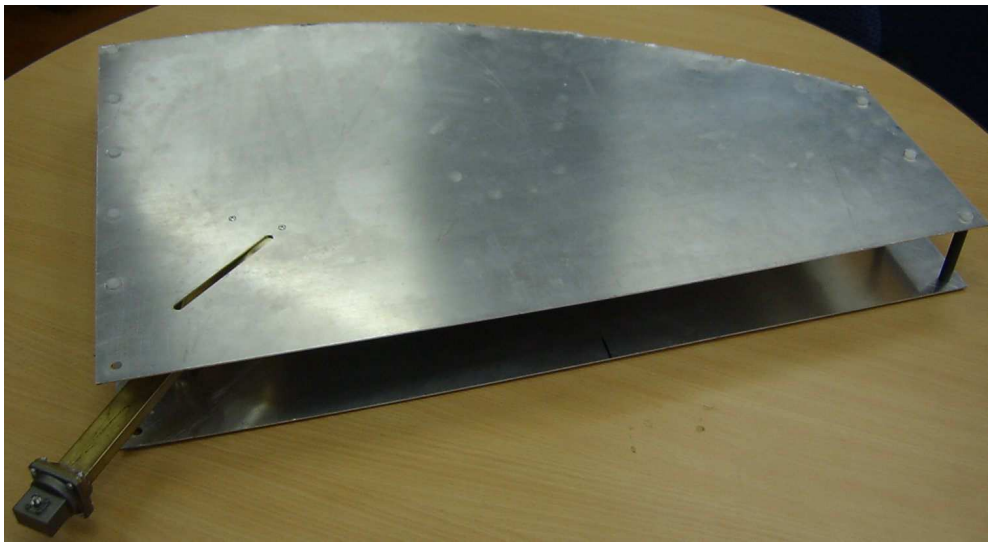

Figure 3.9: Top View of Fully Constructed Antenna

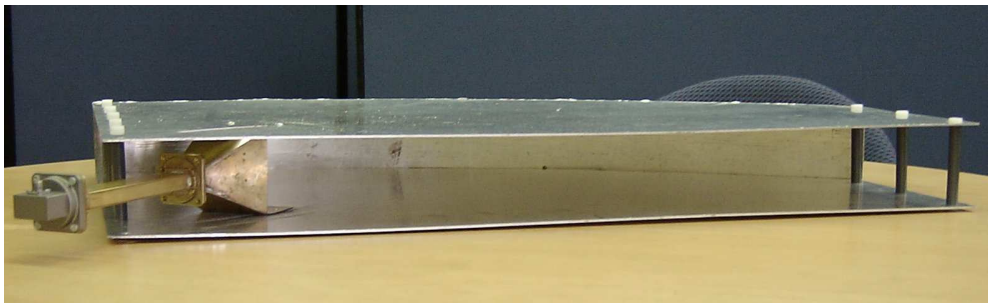

Figure 3.10: Front View of Fully Constructed Antenna

3.6 Conclusion

This chapter discussed the design and construction of the pillbox antenna. The offset-fed antenna was chosen because it avoids aperture blockage and thus lowers sidelobes. The main drawback however has been identified as higher cross-polarization in the plane of offset compared to an axisymmetrically fed antenna. The geometry of the antenna has

been discussed with the main emphasis being the offsetting of the feed to avoid blockage and the feed pointing angle to achieve equal edge illumination.

The dimensions of the pillbox to achieve the desired beamwidths in the principal planes were calculated. The aperture field method was used to simulate the E and H-plane patterns in MATLAB from which the 3 dB beamwidths were predicted. We also computed the directivity of the pillbox antenna.

The feed dimensions in the H-plane to achieve an -10 dB taper at the reflector edges were calculated in MATHCAD and feed horn was constructed from Schelkunoff's equation. The radiation patterns of the feed were also simulated to confirm the -10 dB points as well as predict the half-power points.

The fabrication process and the assembly of the antenna has also been discussed in detail in this chapter.

Chapter 4

Antenna tests & Results

4.1 Introduction

The testing and evaluation of the antenna was performed on the roof of the Menzies building at UCT. To minimise the effects of multipath and distortions, the vicinity of the antennas was kept clear of people and other obstructing objects. The purpose of the tests was to compare the predicted radiation characteristics to the actual radiation characteristics of the antenna.

The far-field of the antenna is calculated using the azimuth dimension:

$$\begin{aligned} \mathrm{R_{ff}} &= \frac{2\mathrm{D}^2}{\lambda} \\ &= \frac{2 \times 56^2}{3.2} \\ &= 19.6 \ [\mathrm{m}] \end{aligned} \tag{4.1}$$

The following measurements and tests were carried for distances greater than or equal to the far-field:

1. Measurement of the feed E and H-plane radiation patterns. Measurement of the -10 dB points of the feed pattern to check if the feed provided proper illumination of the reflector at the edges for an f/D ratio equal to 0.3.

2. The phase centre of the horn was located to provide good illumination of the reflector. The nulls of the pillbox radiation pattern are cleanest and more defined when the feed is properly focused.

3. Measurement of the S_{11} parameter and hence the impedance bandwidth of the antenna.

4. The antenna radiation patterns in the E and H-planes were plotted and the 3 dB beamwidths and sidelobes in the E and H-plane were measured.

5. The gain of the antenna was measured and the radiation efficiency computed.

6. The cross-polarization performance of the antenna was measured and analyzed especially in the offset plane where theoretically the cross-polarization should be significant [25] [28].

4.1.1 Apparatus Used

Below we mention the test equipment that was used for the tests with a short description of each of them:

- Four 50 cm low loss coaxial cables were used to connect the pillbox and the horn to the transmitter and receiver respectively. (Two cables connected in series to provide sufficient length for each connection).

- The HP 8350B sweep oscillator was used to set the transmit frequency at 9.3 GHz CW.

- The HP 8410 A Network Analyzer S parameter test unit is used to determine return loss, S_{11} of the pillbox and the transmission coefficient S_{12} of the connecting cables and these parameters are displayed on the rectangular display module as a function of frequency from 9.25-9.35 GHz.

- HP 83595 RF plug-in unit with an amplitude accuracy of $\pm$1.8 dB was used as the transmitter and connected to the pillbox via a 50 ohm coaxial cable.

- The receiver for the antenna gain measurements and radiation plots was the Agilent E 4407 Spectrum Analyzer (SA).

- A 7.5×5 cm horn antenna was used as the receive antenna for the tests and was connected to the input of the SA.

- A coaxial to waveguide adapter was used to couple the radiation from the pillbox waveguide to the 50 ohm coaxial cables.

- A tripod was used to mount the receive horn and a rotating stand with a protractor was used to mount the pillbox.

- A torque wrench was used for consistent tightening of the SMA connectors to the NA output ports and the SA input ports.

4.1.2 Procedure

All the equipment was turned on and left to warm up for about 30 minutes and once stable tests and measurements were carried out in the following order:

1. Once the receive antenna was connected to the SA we noted the ambient radiation level, which was the noise floor of our receiver system. Since the input signal was CW we set the IF bandwidth (resolution bandwidth) of the spectrum analyzer to 10 kHz and the video bandwidth to 10 kHz for maximum measurement sensitivity. Setting the video bandwidth even lower results in a longer integration time and hence a longer measurement time. A video bandwidth of 10 kHz has an added advantage in that it clarifies the signal trace by smoothing the noise, which yields better measurements for signal levels near the noise floor of the receiver.

2. The transmitter was connected directly to the input of the SA to check if the transmitter was transmitting the specified power. The output of the signal generator must be less than 0 dBm whenever it is connected to the input of the SA otherwise the SA could be damaged.

3. The pillbox (AUT) and the horn antenna were placed 20 m apart at far-field facing one another and at the same height. The AUT boresight was determined by scanning through peak to 3 dB points and then bisecting to find the peak. This was done for both horizontal and vertical polarization.

4. In the H-plane the antenna pattern was plotted for angular increments of 1° and the pattern was measured within the main beam and the first two sidelobes. The E-plane measurements were carried out for angular increments of 5° off boresight. It is important to note that the AUT and the horn had the same polarization for each of the antenna pattern with the exception of the cross-polar patterns where the antennas were orthogonal to one another.

5. Nulls and peaks in the radiation patterns are easily missed and more measurements were taken at the critical angles to get the appropriate patterns [2].

6. The transmitted power of the system was measured after the measurement to determine any uncertainties in readings. The spectrum analyzer has a built-in amplitude uncertainty of ± 0.4 dB.

4.1.3 Precalculations

Expected Receive Power for Antenna Measurements

We used the Friis equation to predict the expected receive power level for boresight measurements at a far-field distance of 20 m and for a transmit power of 20 dBm. Note

that the actual $\mathrm{P_t}$ measured at the transmitter was 19 dBm and the loss in the cables was 2 dB, therefore the power supplied to the antenna terminals was 17 dBm.

$$\begin{aligned} \mathrm{P_r} &= \frac{\mathrm{P_t G_t G_r \lambda^2}}{(4\pi \mathrm{R})^2} \\ &= \frac{50 \times 10^{-3} \times 363 \times 32.21 \times (3.2 \times 10^{-2})^2}{(4\pi \times 20)^2} \\ &\approx -20 \ \text{[dBm]} \end{aligned} \tag{4.2}$$

Therefore we expect a receive power in the region of -20 dBm at the receiver. $\mathrm{G_t}$ was estimated from the directivity of the pillbox.

Prediction of Nulls and Peaks for the Feed:

For the E-plane pattern:

- The nulls occur at [2]:

$$\theta_\mathrm{n} = \arcsin\left(\frac{\mathrm{n}\lambda}{\mathrm{b_1}}\right) \quad \text{where n} = 1, 2, 3, ... \tag{4.3}$$

- The peaks occur at [2]:

$$\theta_\mathrm{p} = \arcsin\left(\frac{1.43\mathrm{n}\lambda}{\mathrm{b_1}}\right) \quad \text{where n} = 1, 2, 3, ... \tag{4.4}$$

For the H-plane pattern :

- The nulls occur at [2] :

$$\theta_\mathrm{n} = \arcsin\left(\frac{1.49\mathrm{n}\lambda}{\mathrm{a_1}}\right) \quad \text{where n} = 1, 2, 3, ... \tag{4.5}$$

- The peak occur at [2]:

$$\theta_\mathrm{p} = \arcsin\left(\frac{1.88\mathrm{n}\lambda}{\mathrm{a_1}}\right) \quad \text{where n} = 1, 2, 3, ... \tag{4.6}$$

The nulls and the peaks of the pillbox power pattern were derived from the MATLAB simulation in Figure 3.3.

4.1.4 Antenna Focus Adjustments

In practice the phase centre of the horn needs to coincide with the focal point of the pillbox to provide good illumination of the reflector. The phase centre of the horn is usually not located at the mouth (throat) but between the imaginary apex and its aperture and for smaller flare angles $(< 20°)$ it moves closer to the aperture [2]. The pillbox was connected to the SA and the horn was connected to the transmitter in the far-field. Both the receive horn and the pillbox had the same polarization. The parabolic reflector was focused by slowly moving the feed horn in and out along the axis of the feed till we registered peak power at the receiver. We also looked at the sidelobe structure to check if the sidelobes were clearly defined, then adjusted for the lowest sidelobes and the deepest nulls we could achieve.

4.2 Measurement Results

4.2.1 Measured E and H-plane Feed Patterns

Table 4.1 shows the recorded E-plane receive power levels at 5 degree angular increments. The protractor used for the measurements had a $\pm 0.5°$ accuracy and the power amplitude uncertainty was ± 0.4 dB.

Table 4.1: **Feed E-plane Power Measurements**

Power /(dBm)	Angle /(degrees)	Power /(dBm)	Angle /(degrees)
-22.22	0	-22.40	-5
-23.08	5	-23.67	-10
-23.96	10	-27.24	-15
-27.35	15	-33.08	-20
-32.97	20	-40.15	-25
-39.47	25	null	-27
null	27	-42.26	-30
-42.18	30	-38.36	-35
-38.44	35	-37.00	-40
-36.59	40	peak (-35.73)	-41
peak (-35.62)	41	-39.24	-45
-39.21	45	-43.88	-50
-42.50	50	-48.92	-55
-48.64	55	-51.74	-60
-51.14	60	-62.00	-65
-62.11	65	null	-67
null	67		

Figure 4.1 shows the measured E-plane pattern of the feed horn. The 3 dB beamwidth was $27 \pm 0.5°$ compared to $"26°"$ predicted from the MATLAB simulation of "Figure 3.7".

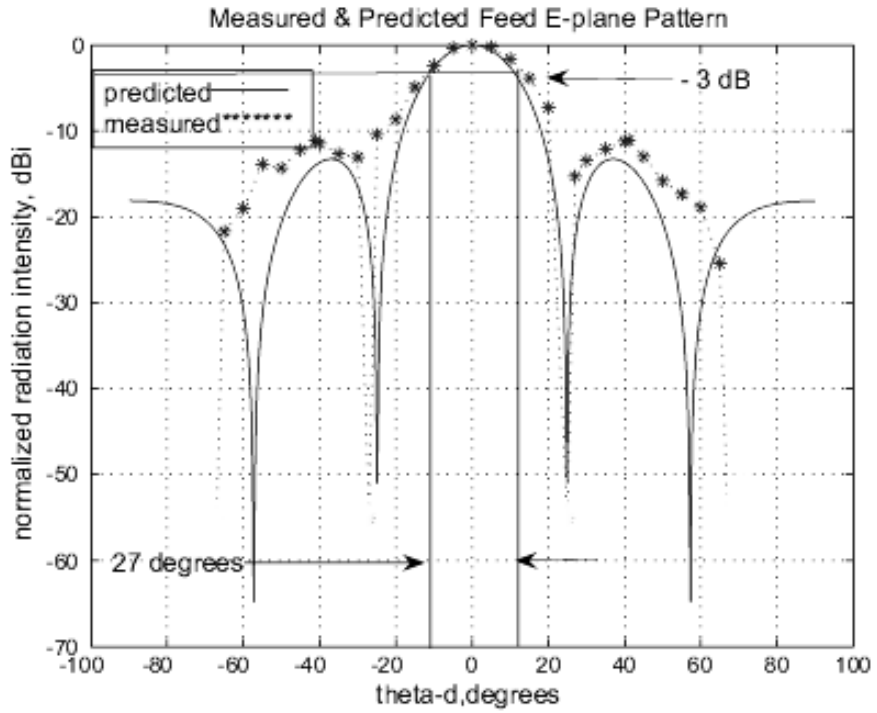

Figure 4.1: Measured & Predicted E-plane Feed Pattern

Table 4.2 below shows H-plane receive power levels at 5 degree angular increments with an uncertainty of $\pm 0.5^{\circ}$ and an amplitude uncertainty of ± 0.4 dB.

Table 4.2: **Feed H-plane Power Measurements**

Power /(dBm)	Angle /(degrees)	Power /(dBm)	Angle /(degrees)
-23.19	0	-23.96	-5
-24.02	5	-24.54	-10
-26.23	10	-25.44	-15
-28.14	15	-26.18	-20
-32.00	20	-33.20	-28
-35.85	25	-35.41	-30
-45.76	30	-42.09	-35
-53.93	35	-55.88	-40
-64.18	40	-64.27	-45
-61.64	45	null	-47
null	47	-61.34	-50
-61.64	50	-54.27	-55
-53.99	55	-51.50	-60
-50.51	60	-48.12	-65
-47.79	65	peak (-46.45)	-68
peak (-47.33)	68	-47.54	-70
-48.33	70	-48.24	-75
-49.61	75		

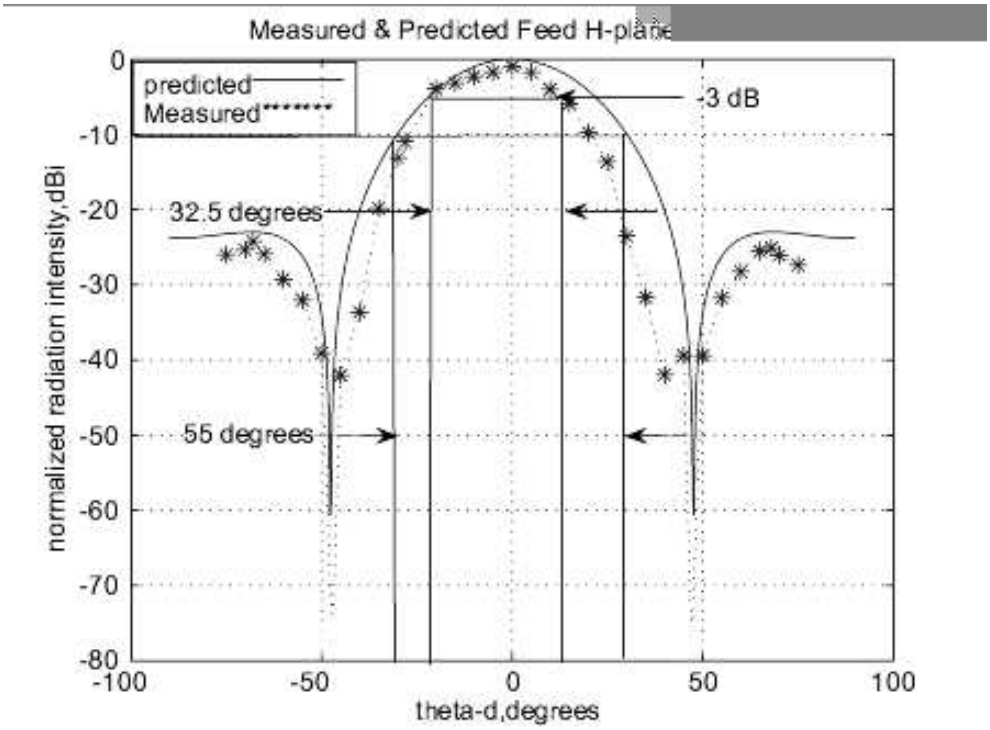

Figure 4.2: Measured & Predicted H-plane Feed Pattern

Figure 4.2 shows the measured H-plane Pattern of the feed horn. The 3 dB beamwidth was $32.5 \pm 0.5^{\circ}$ compared to the predicted beamwidth of 37°in "Figure 3.7", and the measured 10 dB beamwidth of the horn was measured to be $55 \pm 0.5^{\circ}$ compared to the predicted value of 60°.

4.2.2 Return loss Measurement

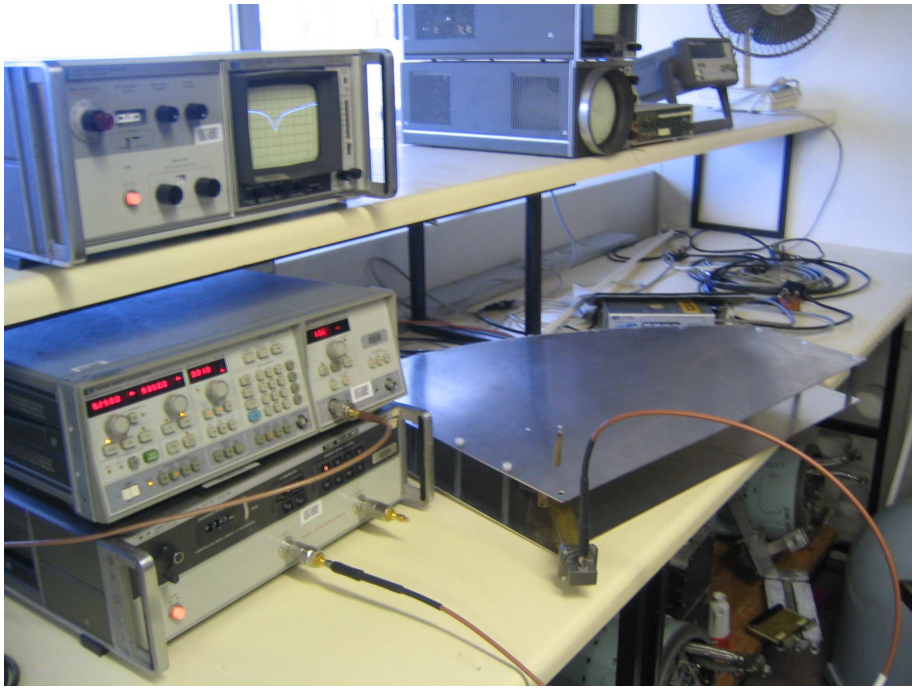

Figure 4.3: Experimental Setup for RL Measurement

The return loss or S_{11} is indicative of the fraction of the incident power reflected back to the feed over a frequency range of measurement and is given by [4]:

$$\begin{aligned} \mathrm{RL\,(dB)} &= -20\log\mid\tau\mid \\ &= 20\log\left|\frac{1}{S_{11}}\right| \end{aligned} \tag{4.7}$$

The Voltage Standing Wave Ratio is the ratio of the maximum to minimum voltage along a transmission line. A $\mathrm{VSWR} \leq 2$ which corresponds to $|\tau| \leq \frac{1}{3}$ constitutes a good impedance matching over the operating frequency and the relationship between VSWR and τ is given by the following equation [4]:

$$|\tau| = \frac{\mathrm{VSWR}-1}{\mathrm{VSWR}+1} \tag{4.8}$$

The impedance bandwidth of the antenna was calculated for a $\mathrm{VSWR} \leq 2$.

The power coupled to the antenna is given by [4] [8] [24]:

$$\mathrm{P_t} = \mathrm{P_{in}}\left(1-\mid\tau\mid^2\right) \tag{4.9}$$

Where $\mathrm{P_t}$ is the power transmitted to the antenna terminals.

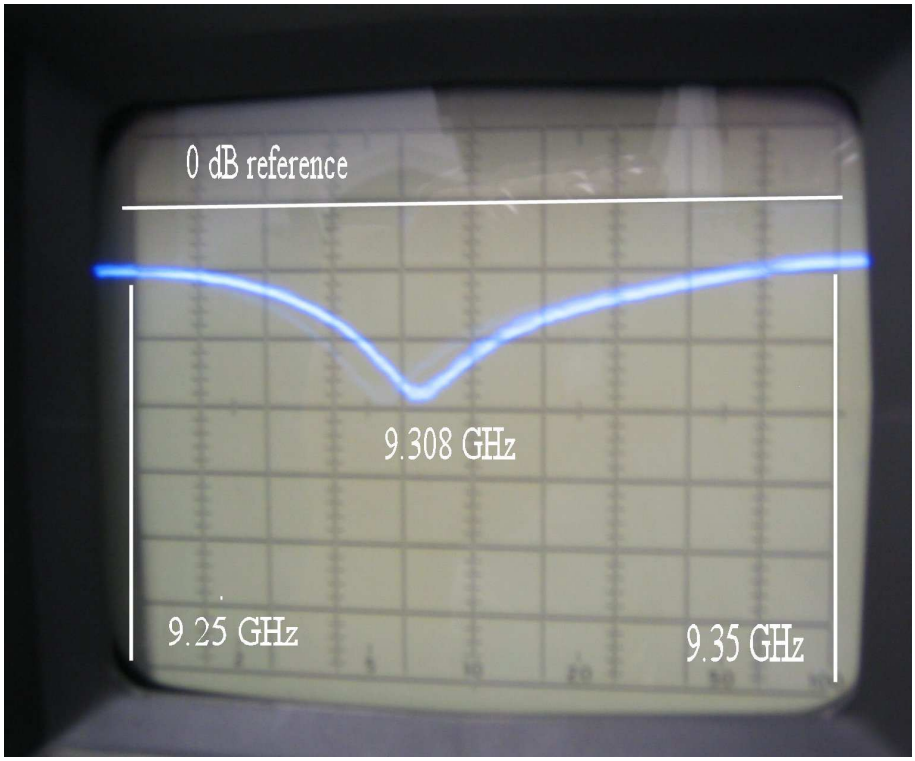

Figure 4.4: Return Loss Plot

Calibration of the Network Analyzer

The amplitude calibration of the NA was done by connecting an SMA short circuit to port 1 and setting the S parameter test set to S_{11}. We adjusted the amplitude vernier so that the trace was directly above one of the division lines and then adjusted the amplitude test set gain so that the trace is on the first division line on the top of the screen.

Return loss of Connecting Cables

- When the coaxial cables were terminated by a matched load (an SMA 50 ohm termination) the return loss of each of them was measured to be more than 20 dB in the 100 MHz bandwidth. That reading was consistent with our expectations.
- When the coaxial cables were terminated by an open circuit, the return loss of each of them in the 9.25 to 9.35 GHz band was measured to be approximately 2 dB. We therefore adjusted the magnitude offset to make the reflection coefficient equal to 0 dB before measuring the return loss of the pillbox antenna.

Insertion Loss of Connecting Cables

- The total insertion loss of the connecting cables due to conductor losses and output mismatch losses was measured and found to be 2 dB.

Return Loss of Antenna

There was a good impedance match between the transmitter and the antenna for a return loss of 10 dB or more in the 100 MHz (9.25-9.35 GHz) frequency band of interest. The impedance bandwidth was measured from figure 4.4 and found to be approximately 100 MHz which was the same as the transmitter bandwidth.

4.2.3 Power Gain of the Pillbox

Since we did not possess a standard gain horn, the power gain of the receive horn was approximated from its dimensions. The aperture efficiency factor is $1/\sqrt{2}$ if we assume no phase variation across the mouth [18]. The frequency dependency of the horn antenna gain and the Schelkunoff ripple effect were disregarded :

$$\begin{aligned} \mathrm{G_r} &= \frac{4\pi \mathrm{A_e}}{\lambda^2} \\ &= \frac{4\pi \times 0.075 \times 0.05 \times 1/\sqrt{2}}{0.032} \\ &= 15.1 \pm 0.1 \ \ [\mathrm{dBi}] \end{aligned} \tag{4.10}$$

Where the gain is calculated to 0.1 dB accuracy from its known dimensions according to [2] [6] [17].
We calculated the power gain using equation 4.9 [11][2]:

$$\mathrm{G_{t\ dB}} = 20\log_{10}\left(\frac{4\pi \mathrm{R}}{\lambda}\right) + 10\log_{10}\left(\frac{\mathrm{P_r}}{\mathrm{P_t}}\right) - \mathrm{G_{r\ dB}} \tag{4.11}$$

Where

$$\begin{aligned} \mathrm{G_{t\ dB}} &= \text{gain of transmitting antenna } [\mathrm{dB}] \\ \mathrm{G_{r\ dB}} &= \text{gain of receiving antenna } [\mathrm{dB}] \\ \mathrm{R} &= \text{antenna separation } [\mathrm{m}] \\ \lambda &= \text{operating wavelength of antenna } [\mathrm{m}] \\ \mathrm{P_r} &= \text{received power } [\mathrm{W}] \\ \mathrm{P_t} &= \text{transmitted power } [\mathrm{W}] \end{aligned}$$

We use the Friis equation for a far-field distance of 20 m with a transmit power equal to 20 dBm. We account for all the losses in the measurement system prior to and after taking

measurements before calculating the power gain of the antenna. The losses are shown in the loss budget table 4.3.

Table 4.3: **Losses in Measurement System**

Loss of transmitter (measured before and after experiment)	1 dB
Insertion loss of transmitting cable	2 dB
Insertion loss of receiving cable	2 dB

The power gain is given as the following, taking into account the transmitter and cable losses;

$$\begin{aligned} \mathrm{G} &= 20\log_{10}\left(\frac{4\pi \mathrm{R}}{\lambda}\right) + 10\log_{10}\left(\frac{\mathrm{P_r}}{\mathrm{P_t}}\right) - \mathrm{G_{r\ dB}} \\ &= 20\log\left(\frac{4\pi \times 20}{0.032}\right) + 24.32 - 17 - 15.1 \\ &= 24 \pm 0.5 \ \ [\text{dBi}] \end{aligned} \tag{4.12}$$

Where the total uncertainty is the sum of the uncertainties associated with $\mathrm{G_r}$ and $\mathrm{P_r}$. The other quantities in the equation above were measured accurately before and after the experiments and they stayed the same.

Antenna Radiation Efficiency

The radiation efficiency of the antenna was computed from equation 2.5 as follows:

$$\begin{aligned} \epsilon_{\mathrm{L}} &= \frac{\mathrm{G_p}}{\mathrm{G_d}} \\ &= \frac{251}{363} \\ &= 0.69 \end{aligned} \tag{4.13}$$

Where
The directivity, $\mathrm{G_d}$ was approximated from equation 2.7.

4.2.4 Measured E and H-plane Patterns of the Pillbox

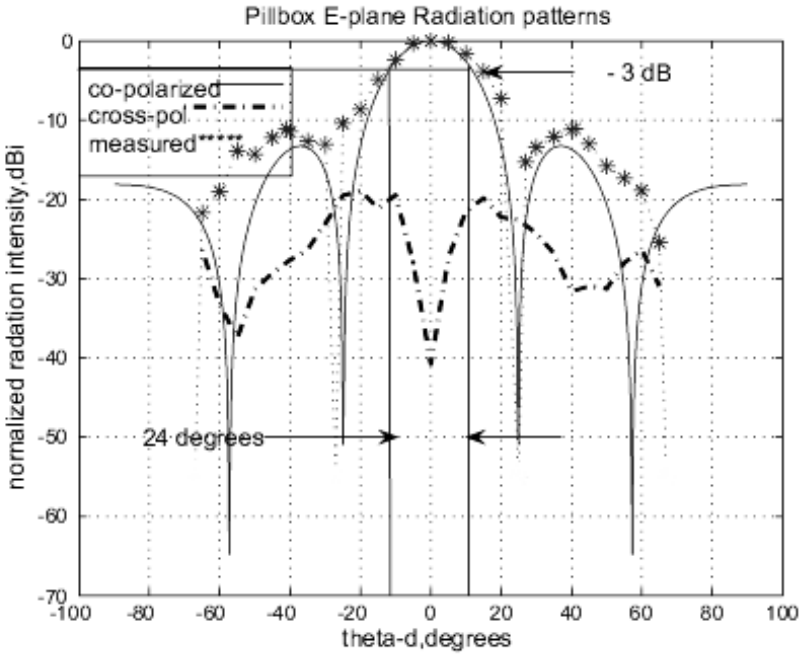

Figure 4.5: E-plane Co-polar Performance of Pillbox (dB w.r.t peak gain)

Figure 4.5 shows the measured E-plane co-polarized pattern as well the cross-polarized pattern. The measured pattern is shown as annotated points in the figure. The 3 dB beamwidth was measured and found to be $24 \pm 0.5^\circ$ in comparison to the predicted value of 25°. The first sidelobe level was found to be approximately -11 dB. The antenna offers good cross-polarization rejection in the E-plane (levels less than -30 dB) within 20° of the beam peak. The peak cross-polarization level was limited to about -22 dB relative to the peak of the main beam in the E-plane. The noise floor of the receiver was approximately -80 dBm (-60 dB relative to the peak of the main beam co-polarized level).

Table 4.4: **E-plane co-pol Power Measurements of Pillbox**

power (dBm)	Angle (degrees)	Power (dBm	Angles (degrees)
-24.91	0	-25.23	-5
-25.12	5	-27.30	-10
-26.53	10	-29.80	-15
-28.78	15	-33.56	-20
-32.18	20	-35.31	-25
-35.43	25	null	-27
null	27	-37.97	-30
-40.19	30	-37.56	-35
-38.34	35	-36.38	-40
-37.00	40	-36.02 (peak)	-41
peak (-36.13)	41	-37.13	-45
-36.00	45	-39.21	-50
-37.91	50	-38.78	-55
-40.72	55	-43.91	-60
-42.25	60	-46.64	-65
-43.77	65	null	-67
-80	67		

Table 4.5: **E-plane X-pol Power Measurements of Pillbox**

Power (dBm)	Angle (degrees)	Power (dBm)	Angle (degrees)
-65.63	0	-52.84	-5
-52.26	5	-44.36	-10
-46.36	15	-46.00	-15
-44.75	20	-43.80	-20
-47.15	25	-44.42	-25
-47.47	30	-47.94	-30
-49.19	35	-51.24	-35
-51.74	40	-52.55	-40
-56.51	45	-54.19	-45
-55.82	50	-56.25	-50
-56.18	55	-62.35	-55
-52.89	60	-58.21	-60
-55.82	65	-51.23	-65

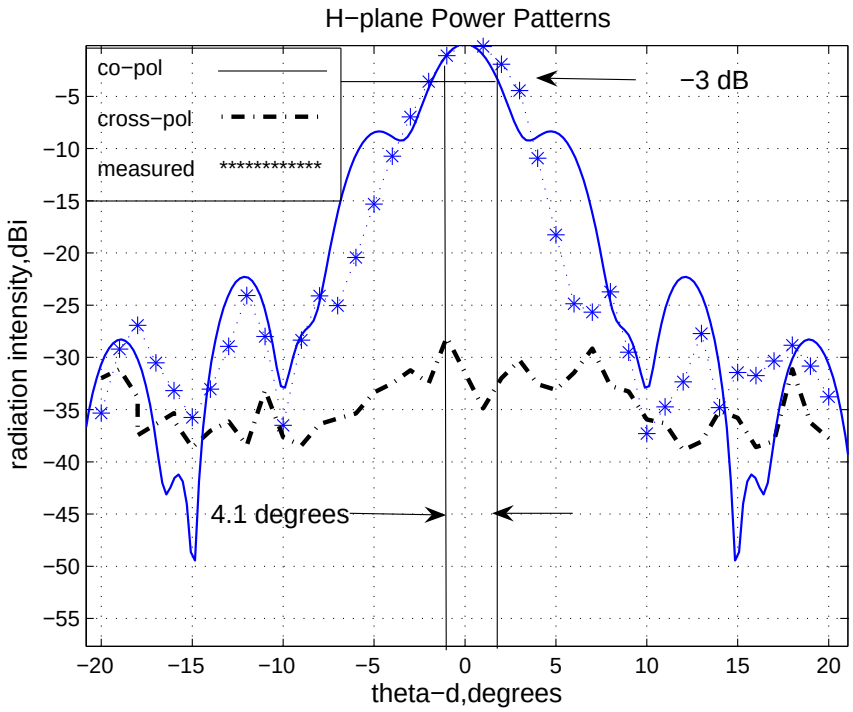

Figure 4.6: H-plane Co-polar Performance of Pillbox (dB w.r.t peak gain)

Figure 4.6 shows the measured H-plane pattern and the cross polarization performance. The measured pattern is shown as annotated points in the figure. The 3 dB beamwidth was measured and found to be $24 \pm 0.5°$ in comparison to the MATLAB prediction of -23 dB. The measured H-plane 3 dB beamwidth was found to be $4.1°$ in comparison to the predicted value of $3.8°$. This is justified since a wider beam implies lower sidelobes due to the taper imposed on the reflector edges. A maximum cross-polarization level of -28 dB occurred $-3°$ off the peak of the main beam. The cross-polarization rejection was generally quite good within $20°$ of the beam peak (less than -30 dB relative to the peak of the main beam). The noise floor of the receiver was approximately -77 dBm (about 50 dB below the peak of the co-polarized pattern).There is however, a discrepancy between the general shape of the predicted and the measured H-plane patterns. Both Figure 4.6 and Figure 3.2 have nulls at $\pm 10°$, $\pm 15°$ $\pm 20°$ but the measured pattern has a 10 dB beamwidth of $8°$ while in the predicted pattern it is $12°$. This could be due to improper focusing of the feed.

Table 4.6: **H-Plane Co-polar Power Peasurements of Plllbox**

Power (dBm)	Angle (degrees)	Power (dBm)	Angle (degrees)
-24.34	0	-25.44	-1
-24.56	1	-27.93	-2
-26.26	2	-31.31	-3
-28.78	3	-35.08	-4
-35.26	4	-39.66	-5
-42.61	5	-44.77	-6
-49.20	6	-49.37	-7
-50.00	7	-48.45	-8
-48.07	8	-52.68	-9
-53.84	9	-60.85	-10
-61.64	10	-52.34	-11
-59.07	11	-48.41	-12
-56.67	12	-53.29	-13
-52.06	13	-57.37	-14
-59.15	14	-60.1	-15
-55.79	15	–57.51	-16
-56.08	16	-54.85	-17
-54.68	17	-51.27	-18
-53.18	18	-53.54	-19
-55.18	19	-59.67	-20
-58.12	20		

Table 4.7: **H-plane X-pol Power Measurements of Pillbox**

Power (dBm)	Angle (degrees)	Power (dBm)	Angle (degrees)
-52.39	0	-56.80	-1
-59.20	1	-55.56	-2
-56.31	2	-56.80	-3
-54.59	3	-57.68	-4
–56.88	4	-59.68	-5
-57.43	5	-60.17	-6
-55.79	6	-60.70	-7
-53.48	7	-62.75	-8
-57.04	8	-61.97	-9
-57.59	9	-57.45	-10
-60.26	10	-62.75	-11
-60.64	11	-60.45	-12
-63.21	12	-61.35	-13
-62.38	13	-62.94	-14
-59.42	14	-60.39	-15
-60.11	14	-59.65	-16
-62.91	15	-61.77	-17
-62.33	17	-58.13	-18
-55.45	18	-55.45	-19
-60.56	19	-56.31	-20
-62.06	20		

4.3 Conclusion

This chapter gave a description of the type of testing that was performed to evaluate the performance of the antenna. The equipment used for the tests was discussed in detail. The return loss of the antenna was measured. The E and H-plane patterns of the antenna were measured and the 3 dB beamwidths were also measured. The cross-polarization performance of the antenna was also measured.

Results from the antenna tests were analyzed and compared to MATLAB and theoretical predictions. All sources of error and uncertainties associated with the measurements were identified and accounted for. System losses which included cable losses were recorded.

In summary the pillbox performed well within the specifications set out in Section 1.2. The 3 dB beamwidth of the H-plane co-polar pattern was measured to an accuracy of 0.1° and found to be 4.1°compared 3.8°predicted from the MATLAB simulation in Figure 4.6. The first sidelobe level was approximately -24 dB relative to the beam peak. The measured E-plane beamwidth was $24^\circ$and the uncertainty in the measurement was $\pm 1^\circ$.The MATLAB simulation of Figure 4.5 predicted an E-plane beamwidth of 25°. The first time sidelobe level was -11 dB relative to the peak in the E-plane pattern. The power gain of

the antenna was calculated to be 24 ± 0.5 dBi.

The slightly wider H-plane measured beamwidth could have been due to improper focussing of the feed. The feed exhibits both lateral and axial movement as it is moved back and forth in trying to locate the phase centre. A remedy to this might be to have the slot of FACE PLATE-1 (See APPENDIX. B) running parallel to the reflector axis. This allows axial focussing whilst simultaneously allowing the feed to rotate to the correct position on the offset parabola. There is also a discrepancy between the general shape of the predicted and the measured H-plane patterns. Even though both Figure 4.6 and Figure 3.2 have nulls at $\pm 10°$, $\pm 15°$ $\pm 20°$, the measured pattern has a 10 dB beamwidth of $8°$ while in the predicted pattern it is $12°$. This discrepancy could be due to a quadratic phase error at the aperture of the pillbox or an error in programming Equation 9 to obtain the predicted radiation pattern.

The structural changes as well as the improved testing methods mentioned above should go a long way in improving the performance of the antenna as a whole.

Chapter 5

Conclusions & Recommendations

5.1 Conclusions

The objectives of this dissertation have been to design, implement and test the radar antenna for SASARII according to specifications given in Section 1.2 of the dissertation. This objective was met as a whole and based on the findings and the experimental results, the following conclusions are drawn:

1. The radiation patterns of the antenna in the E and H-plane were successfully simulated and the 3 dB beamwidths in the E and H-planes were shown to be 25° and 3.8° respectively. The sidelobe levels for the E and H-plane were 13 dB and 23 dB respectively. The directivity of the antenna was calculated and found to be 25.6 dBi.

2. The antenna and feed geometry were calculated and CAD drawings were made from which the antenna and the feed horn were fabricated.

3. Antenna tests were carried out and the results recorded. All error sources were accounted for and the uncertainties in measurements and calculations were recorded. The antenna was well matched to the transmitter with an impedance bandwidth of 100 MHz which was determined from the S_{11} test. A special method using a laser pointer was used to precisely determine the narrow beamwidth in the H-plane (See APPENDIX C). The 3 dB beamwidth of the H-plane co-polar pattern was measured to an accuracy of 0.1° and found to be 4.1°. The first sidelobe level was approximately -24 dB relative to the beam peak. The measured E-plane beamwidth was $24^\circ$and the uncertainty in the measurement was $\pm 1^\circ$. The first time sidelobe level was -11 dB relative to the peak in the E-plane pattern. The power gain of the antenna was calculated to be 24 ± 0.5 dBi. The slightly wider H-plane measured beamwidth could have been due to improper focussing of the feed. The feed exhibits both lateral and axial movement as it is moved back and forth in trying to locate the phase centre.

4. The cross-polarization performance in the H-plane was satisfactory and acceptable within 20° of the main beamwidth, levels were generally less than - 30 dB relative to the peak of the main beam. In the E-plane we expected good cross-polarization rejection at the peak of the E-plane which was the case where the cross-pol level was close to the noise floor of the receiver (approximately -80 dBm).

5.

In summary, a prototype of the radar antenna has been designed and fabricated and the results of tests carried out suggest that the antenna's performance is satisfactory and within the specifications.

5.2 Recommendations

1. Reflections from the ground and walls might have contributed to the level of cross-polarization in the antenna patterns. A slant range could improve the X-pol measurements because reflected signals are suppressed.

2. A test range with a better controlled environment to minimise obstruction and electromagnetic interference as well as automated test equipment for more accurate measurements. A fully instrumented test range would enable the investigation of the effect of closing the sidewalls with solid metal walls. A flat sheet microave absorber can be used suppress any internal reflections.

3. The horn dimension in the azimuth plane was found to be 0.5 cm wider due to an error in the initial calculation. This could have explained the slightly larger H-plane beamwidth of the pillbox and lower sidelobe levels than the expected ones due to under illumination.We can investigate this effect my computing the H-plane pattern using Equation 2.11 and seeing the effect on the edge taper. In addition FEKO software could be used to analyze the co-pol and x-pol performance in the antenna.

4. The method used to measure the pattern only made point measurements, therefore for a continuous pattern there is need for better interpolation. A continuous pattern recorder could be used for this.

5. Due to the snug fitting of the horn inside the pillbox it was not always easy to smoothly move it in and out to locate the phase centre. Further tests are suggested to confirm the best position for the feed focus, these tests can be time consuming and need patience and skill. The antenna pattern would be defined more as a result of locating the the right position of phase centre. In future a technique for making focussing adjustments must be devised so that axial and transverse movements of the feed are independent.

6. The polarization characteristics of the feed horn need to be investigated to determine how much they contribute to the measured X-pol levels of the pillbox.

Appendix A

Software Source Code

A.1 Ray Tracing Code

```
%-------------------------------------------------------------------------
% H-plane feed pattern
%-------------------------------------------------------------------------
%constants
clc
lam=0.032;% operating wavelength in ’m’
k=2*pi/lam;% wave number
E0=1;Aperture E-field in ’V/m’
a=0.065 % horn azimuth dimension in ’m’;
theta=(-400:400)*pi/800;
theta_offset=(45.5/180)*pi; % feed pointing angle
theta_d= theta*180/pi;
dd=-a/2:a/800:a/2;% aperture length
aa1=zeros(1,801);
aa2=zeros(1,801);
aa3=zeros(1,801);
F_2=zeros(1,801);
aa3=(E0*cos(pi.*dd/a))% Horn aperture field distribution;

for i=1:801


    aa1(i)=sum((aa3/lam).*cos(k*sin(theta(i)-theta_offset)*dd)*0.001);
    aa2(i)=sum((aa3/lam).*sin(k*sin(theta(i)-theta_offset)*dd)*0.001);

end

aa=aa1 + j*aa2; % Complex fourier transform:  feed E-field
F_1=abs(aa)/max(abs(aa));% normalized feed far field pattern
```

```
F_2= F_1.^2; % directive gain
F_dB=20*log10(F_1); % normalized directive gain

plot(theta_d, aa/max(abs(aa)))% Horn radiation pattern;
plot( theta_d, F_dB)% Horn power gain pattern ;grid
xlabel('theta_d,degrees');
ylabel('radiation intensity,dB');
title('H-plane offset feed pattern');
%-------------------------------------------------------------------------
% E-plane pattern for feed and pillbox
%-------------------------------------------------------------------------
%Constants
lam=0.032; % propagation wavelength in 'm'
k=2*pi/lam; % wavenumber.
a=0.07; % E-plane aperture dimension in 'm'.
theta=(-400:400)*pi/800; % theta range.
E0=1; % E-field in 'volts/m'
dd = -a/2:a/800:a/2; aperture length in 'm'
theta_d=theta*180/pi; % theta in degrees.
aa1 = zeros(1,801);
aa2 = zeros(1,801);

for i=1:801

    aa1(i) = sum((E0/lam)*cos(k*sin(theta(i))*dd)*0.001);
    aa2(i) = sum((E0/lam)*sin(k*sin(theta(i))*dd)*0.001);

end

aa = aa1 + j*aa2; % complex fourier transform summation.
F=abs(aa)/max(abs(aa));% normalized radiation pattern.
F_dB=20*log10(F); % normalized radiation pattern in dB.

plot(theta_d,F.^2); grid
xlabel ('theta_d,degrees');
ylabel ('radiation intensity,dB');
title( 'Far field elevation pattern');

%-------------------------------------------------------------------------
% H plane pillbox power pattern
% -------------------------------------------------------------------------
%constants
```

```
lam=0.032 % operating wavelength;
k=2*pi/lam % wavenumber;
E0=1 % E-field in V/m;
f = 0.38; % focal length in ’m’
a=0.065 % feed dimension in ’m’
D_p = 1.26; % parent parabola span
D= 0.56; % reflector span in ’m’
h = D/8; % height of offset in ’m’

theta_a=(-800:800)*pi/1600;
theta_a_d=theta_a*180/pi;
theta=(0:1600)*pi/3200;
theta_off= (49.68/180)*pi % feed pointing angle;
theta_upper= (79.61/180)*pi; %angle subtended by upper edge
theta_lower= (10.58/180)*pi; %angle subtended lower edge
theta_dish=theta_a*(((theta_upper-theta_lower)*180/pi)/90);
theta_d= theta*180/pi;
dd=-a/2:a/1600:a/2; % feed integration subintervals in ’m’
DD= h:((D_p/2-h)/1600):D_p/2; % reflector integration subintervals
in ’m’

aa1=zeros(1,1601);
aa2=zeros(1,1601);
aa3=zeros(1,1601);
SL=zeros (1,1601);
F_2=zeros(1,1601);
aa4=zeros(1,1601);
aa5=zeros(1,1601);
SL=cos(theta_dish/2).^2;
aa3=(E0*cos(pi.*dd/a)); % cosinusiodal E-field distribution in V/m
for i=1:1601


    aa1(i)=sum((aa3/lam).*cos(k*sin(theta(i)-theta_off)*dd)*0.001);
    aa2(i)=sum((aa3/lam).*sin(k*sin(theta(i)-theta_off)*dd)*0.001);

end

aa=aa1 + j*aa2; % Complex fourier transform:  Far-field (E field)
pattern of the aperture.
F_1=abs(aa)/max(abs(aa));% normalized far field strength of the (E
-field) aperture.
F_2= F_1.^2; % normalized E-field squared / power gain of the feed
```

```
aperture
F_dB=20*log10(F_1); % power gain in dB: Normalized E_field squared

plot(theta_d, F_dB);
xlabel('theta_d,degrees'); grid
ylabel('radiation intensity,dB');
title('feed pattern')

%-------------------------------------------------------------------------
% effective aperture field distribution at the reflector
%-------------------------------------------------------------------------
A_field = sqrt((F_2.*SL)./f) ;
A_f_norm = abs(A_field)/max(abs(A_field));

%-------------------------------------------------------------------------
% reflector far field:  Fourier transform of reflector aperture field
%-------------------------------------------------------------------------
for i=1:1601


    aa4(i)=sum((A_f_norm/lam).*cos(k*sin(theta_dish(i))*DD)*0.001);
    aa5(i)=sum((A_f_norm/lam).*sin(k*sin(theta_dish(i))*DD)*0.001);

end

aa6=aa4 + j*aa5; % complex fourier transform of the reflector aperture
field
F_3=abs(aa6)/max(abs(aa6));
F_3_dB = 20*log10(F_3); % directive gain in dB: Normalized E_field
squared of the reflector

figure; plot(theta_a_d,F_3_dB);
xlabel('theta_a_d,degrees'); grid
ylabel('radiation intensity,dB');
title('Far field azimuth pattern:offset feed');
```

A.2 Mathcad Code

The following code was used to calculate the H plane dimensions of the horn to achieve -10 dB taper at the reflector edges.

$a := 0.045 \qquad \lambda := 0.032$

Given

$$\left[\frac{\pi^2 \cdot \cos\left(\frac{\pi \cdot a}{\lambda} \cdot \sin\left(1.10^{-30}\right)\right)}{\pi^2 - 4\left(\pi \frac{a}{\lambda} \sin\left(1.10^{-30}\right)\right)^2}\right]^2 = 1$$

$$\left[\frac{0.8666\,\pi^2 \cos\left(\pi \frac{a}{\lambda} \sin(0.663225)\right)}{\pi^2 - 4\left(\pi \frac{a}{\lambda} \sin(0.663227)\right)^2}\right]^2 = \frac{1}{10}$$

$ratio := \text{MinErr}(a, \lambda)$

$$ratio = \begin{pmatrix} 0.047 \\ 0.03 \end{pmatrix}$$

Appendix B

Antenna CAD

The following pages show the X-Y coordinates of the reflector including CAD drawings of the antenna and the feed horn.

Table B.1: **Reflector X-Y Coordinates**

Angle,degs	$\rho(\psi)$ (mm)	X (mm)	Y (mm)	Angle,degs	$\rho(\psi)$ (mm)	X(mm)	Y(mm)
0	380	380	0	50	462.6	297.4	354.4
11	383.5	376.5	73	53	474.5	285.5	378.9
14	385.7	374.3	93.3	56	487.4	272.6	404.1
17	388.5	371.5	113.6	59	501.6	258.4	430
20	391.8	368.2	134	62	517.2	242.8	456.7
23	395.7	364.3	154.6	65	534.2	225.8	484.2
26	400.3	359.7	175.5	68	552.9	207.1	512.6
29	405.4	354.6	196.5	71	573.3	186.7	542.1
32	411.2	348.8	217.9	74	595.8	164.2	527.7
35	417.8	342.2	239.6	77	620.4	139.7	604.6
38	425.1	334.9	261.7	80	647.6	112.4	637.7
41	433.1	326.9	284.2				
44	442	318	307.1				
47	451.8	308.3	330.5				

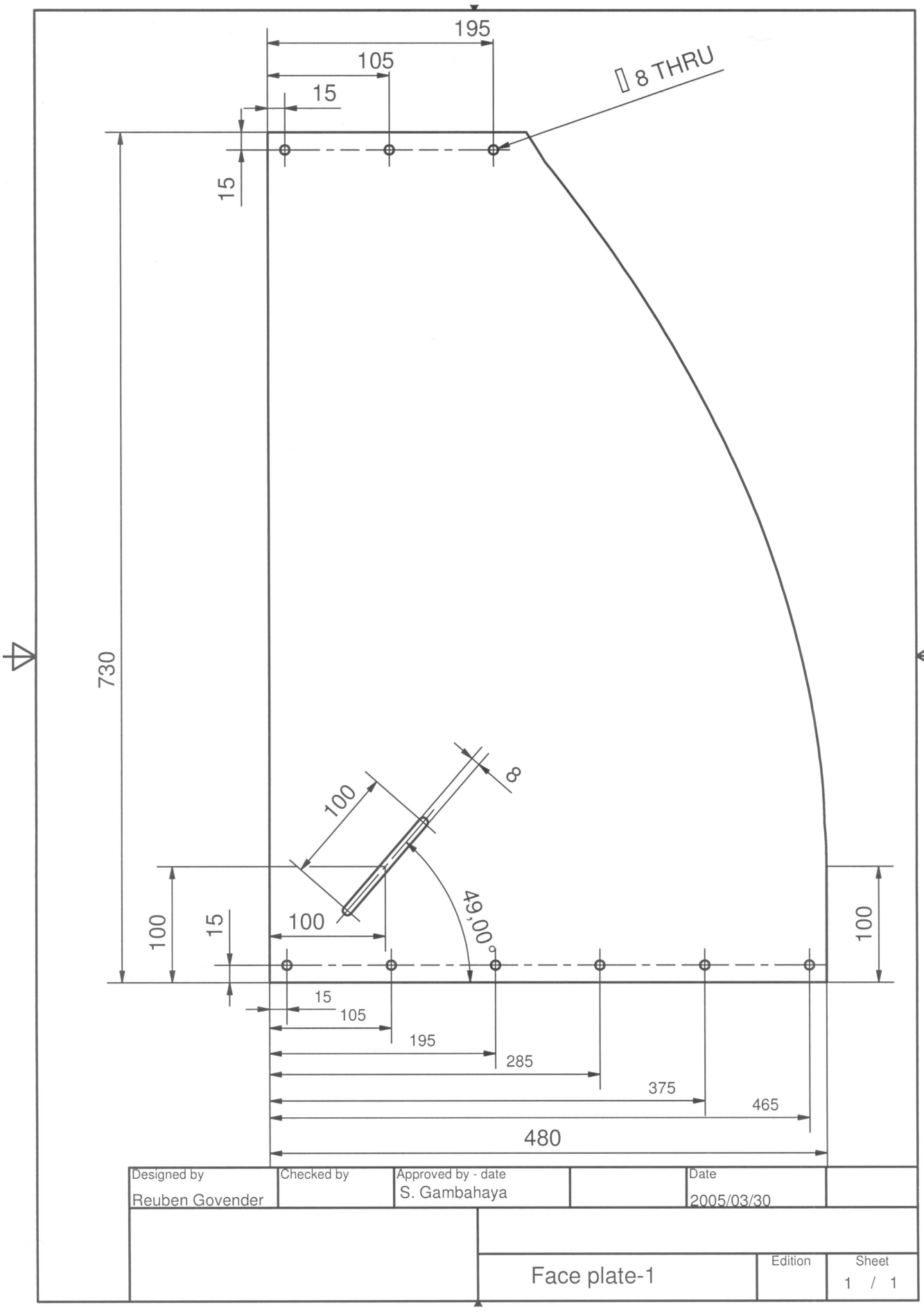
195
105
15
⌀8 THRU
15
730
100
15
100
8
49,00°
100
15
105
195
285
375
465
480
Designed by
Reuben Govender
Checked by
Approved by - date
S. Gambahaya
Date
2005/03/30
Face plate-1
Edition
Sheet
1 / 1

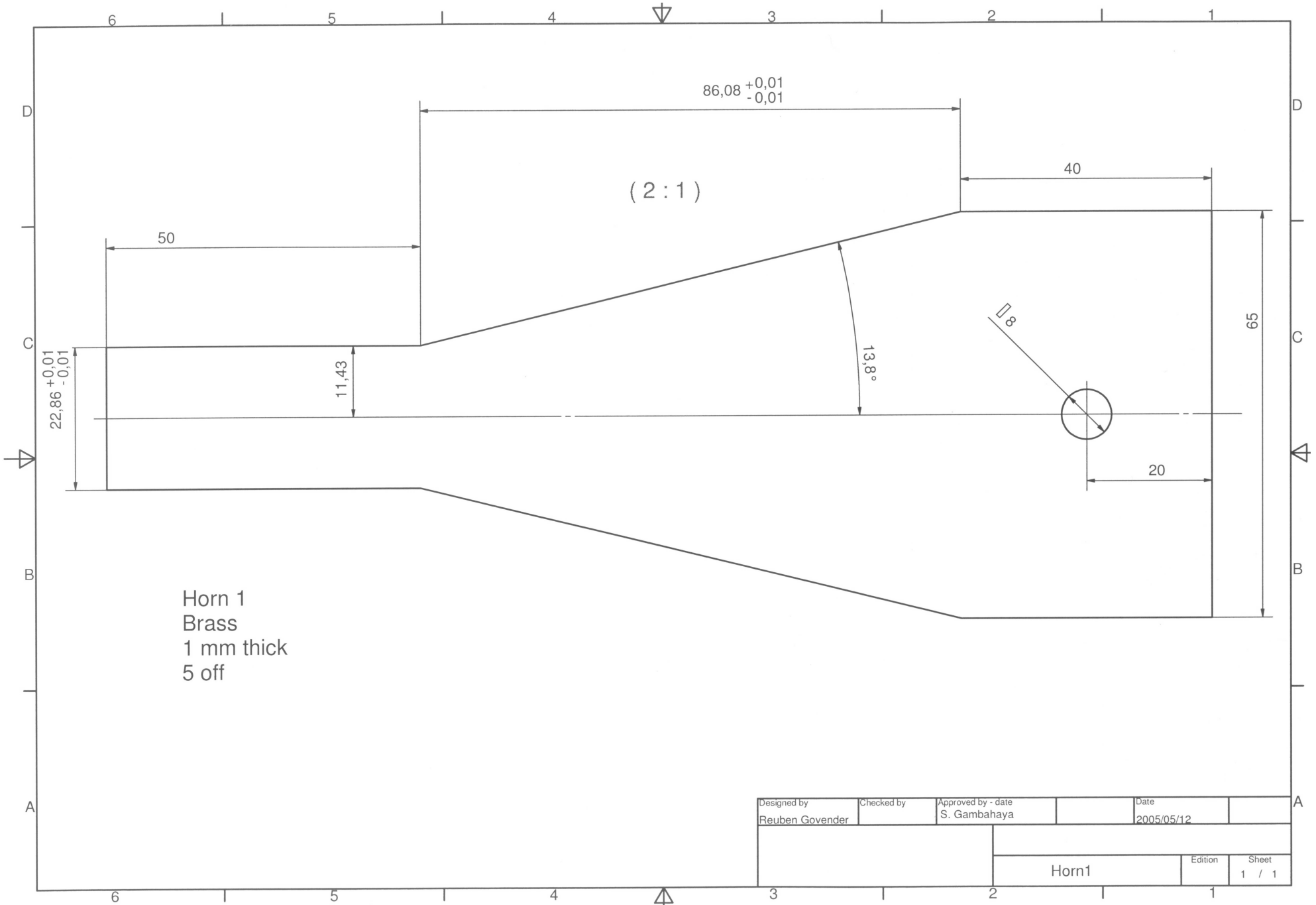
86,08 +0,01 -0,01
(2 : 1)
40
50
65
22,86 +0,01 -0,01
11,43
13,8°
⌀8
20
Horn 1
Brass
1 mm thick
5 off
Designed by
Reuben Govender
Checked by
Approved by - date
S. Gambahaya
Date
2005/05/12
Horn1
Edition
Sheet
1 / 1

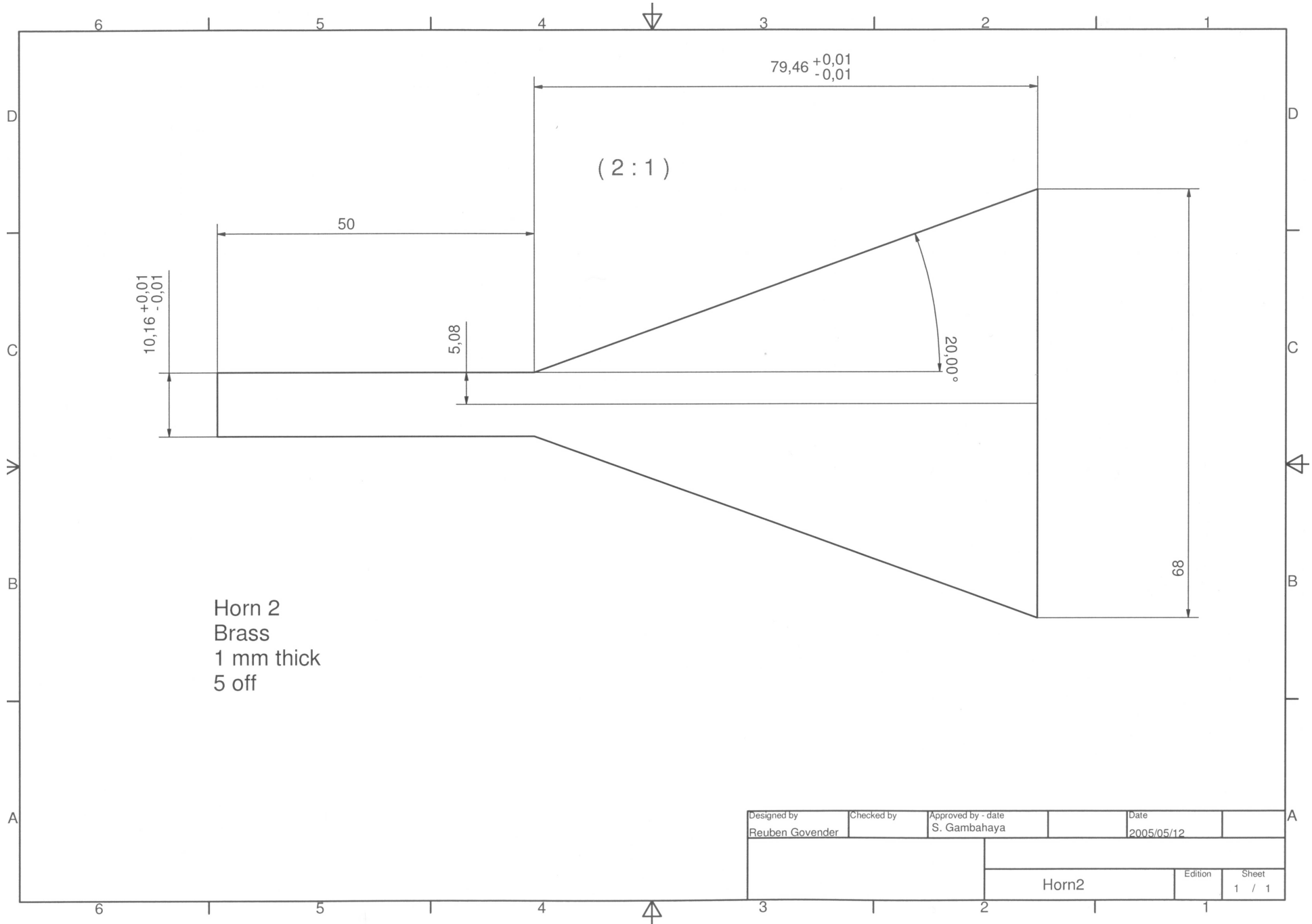
79,46 +0,01 -0,01
(2 : 1)
50
10,16 +0,01 -0,01
5,08
20,00°
68
Horn 2
Brass
1 mm thick
5 off
Designed by
Reuben Govender
Checked by
Approved by - date
S. Gambahaya
Date
2005/05/12
Horn2
Edition
Sheet
1 / 1

Appendix C

Method for Determining H-plane 3 dB Beamwidth

This page explains the method for calculating the 3 dB beamwidth of the antenna in the H-plane to an accuracy of $0.1°$. The user requirements stated a desired azimuth beamwidth of $3.8°$, however since the measurements were carried out manually there was no protractor available that could measure to an accuracy of $0.1°$. The method described below might seem crude but it was quite effective in measuring the H-plane beamwidth. The experiment was performed twice and consistently gave the same results.

C.1 Description

We suggest a method based on the small angle approximation:

$$\mathrm{S} = \mathrm{R}\theta$$

Where

$$\begin{aligned} \mathrm{S} &= \text{arc length=distance between dots} \\ \mathrm{R} &= \text{far-field distance} \\ \theta &= \text{Small angular increment} \end{aligned}$$

This method is justified since θ is very small and R is large. See figure C.2. The figure simply illustrates the concept and is not at all to scale.

A laser pointer was attached to the top plate of the antenna just above the aperture. We scanned through peak power to 3 dB points and then bisected the subtended angle to find the peak. Having located the boresight we marked it on a chart which was placed in the background of the receiver at the same height as the receiver. The laser beam was used to accurately mark off the position of the peak on the background chart (see figure

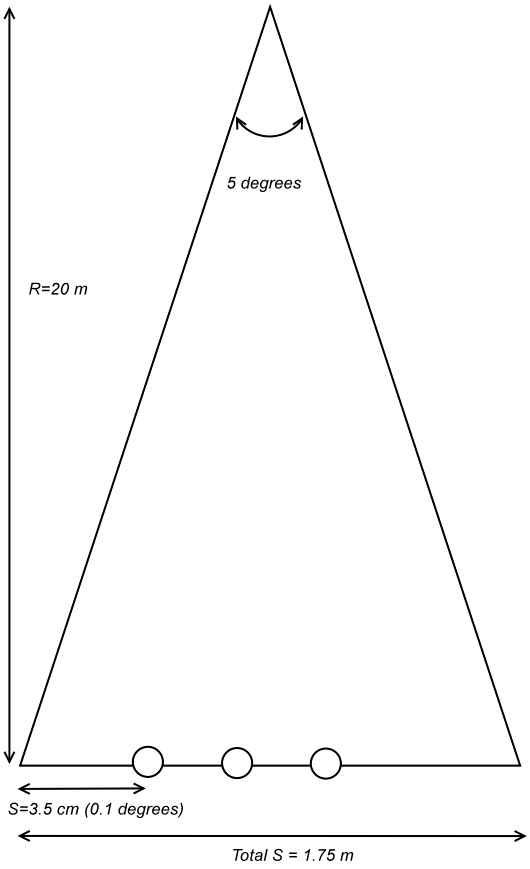

Figure C.1: Construction for Determining 3 dB Points

C.2). With the peak position as reference, the total subtended angle to the 3 dB points was measured by shining the laser to those points and recording the distance between the points.

The distance between the dots corresponding to an angle of 0.1° is given by:

$$\begin{aligned} \mathrm{S} &= \mathrm{R}\theta \\ &= 20 \times \left(\frac{0.1 \times \pi}{180}\right) \\ &= 3.5 \ [\mathrm{cm}] \end{aligned}$$

Using this method the beamwidth was measured accurately to be 4.1°.

Figure C.2: Receive horn with the ‘dotted’ background chart

C.2 Feed Angle for Equal Edge Illumination

This section shows how the feed pointing angle for equal edge illumination was obtained using a graphical method which will be illustrated shortly. The design is based on finding an angle which gives a feed taper imbalance that corresponds to an equal edge illumination. The difference in edge illumination at the edge of the reflector is given by [28] :

$$\Delta\mathrm{EI} \quad = \quad \mathrm{EI_U} - \mathrm{EI_L} \ \ [\mathrm{dB}] \tag{C.1}$$

For a balanced edge illumination $\Delta EI = 0$, therefore equation C.2 can be written as [28]:

$$\mathrm{FT_L} + \mathrm{SPL_U} \quad = \quad \mathrm{FT_L} + \mathrm{SPL_L} \tag{C.2}$$

Substituting SPL into equation C.2 gives

$$\Delta\mathrm{FT} \quad = \quad \mathrm{FT_L} - \mathrm{FT_U} \tag{C.3}$$

$$= \quad 40 \log \left[\frac{\cos \frac{\psi_\mathrm{L}}{2}}{\cos \frac{\psi_\mathrm{U}}{2}} \right]$$

$$= \quad 4.5 \ [\mathrm{dB}]$$

Therefore $\Delta\mathrm{FT} = 4.5$ dB.

The angle between the lower and the upper edge of the reflector is approximately equal to $69°$.

C.2.1 Description

A Small piece of gridded paper is cut out with the same scale as in the feed pattern and with a width of $69°$. The reference points 'O' and $\Delta\mathrm{FT}$ are marked as shown in figure C.3. The marked piece of paper is moved on the feed radiation pattern plot until the points 'O' and $\Delta\mathrm{FT}$ fall on the feed pattern curve. Finally the value of the angle between the pattern peak and the lower edge point $\Delta\mathrm{FT}$, is read from the graph [28] .

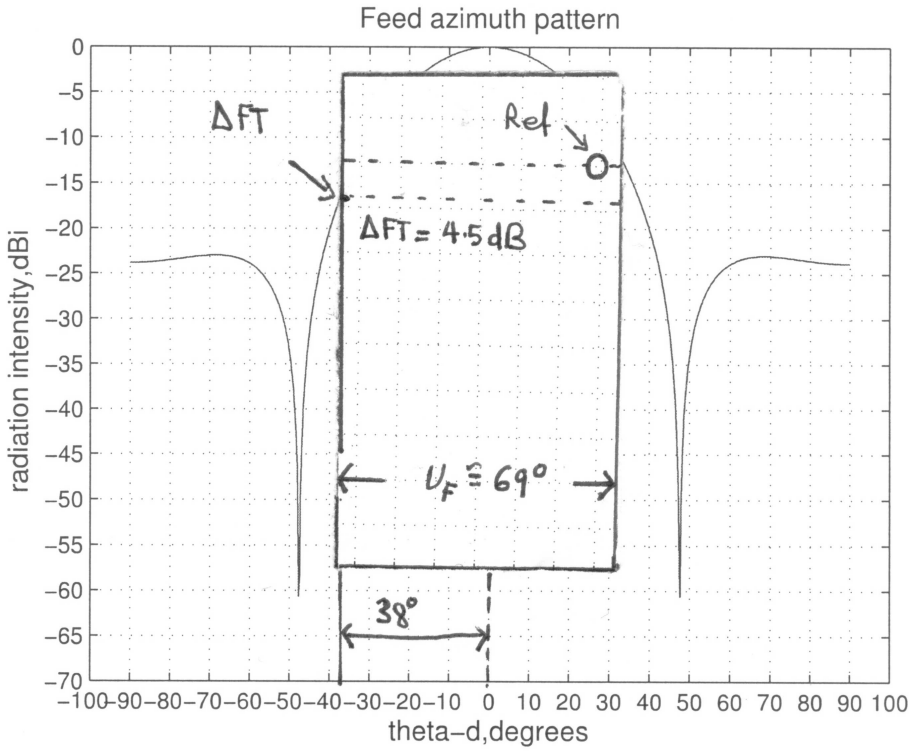

Figure C.3: Feed Pointing Angle for Equal Edge Illumination

The feed pointing angle is then calculated by adding ψ_L to ψ_P. For this antenna the feed pointing angle for equal edge illumination was calculated to be:

$$\begin{aligned} \psi_\mathrm{E} &= \psi_\mathrm{L} + \psi_\mathrm{P} \\ \psi_\mathrm{E} &= 11° + 38° \\ &= 49° \end{aligned} \tag{C.4}$$

Bibliography

[1] *IEEE Standards Online Antennas and Propagation Standards*.

[2] Balanis C A. *Antenna Theory: Analysis and Design*. John Wiley and Sons, 1997.

[3] Bracewell R. *The Fourier Transform and its Applications*. McGraw-Hill Book Company, Jan 1965.

[4] Chang K. *RF and Microwave Wireless Systems*. John Wiley and Sons, 2000.

[5] Cheng D K. *Field and Wave Electromagnetics - 2nd Edition*. Addison-Wesley Publishing Company, Jan 1989.

[6] Clarke R H, Brown J. *Diffraction Theory and Antennas*. John Wiley and Sons, Jan 1980.

[7] Connors F R. *Antennas*. Edward Arnold Herman Publishing Inc., 1972.

[8] Downing B.J. EEE482F RF and Microwave class notes. Used as class notes for UCT students.

[9] Elliott R S. *Antenna Theory and Design*. Prentice Hall, Jan 1981.

[10] Harris F J. On the Use of Windows for Harmonic Analysis with the Discrete Fourier Transform. *IEEE Proceedings*, 66(1):51–83, Jan 1978.

[11] Hollis J.S. *Microwave Antenna Measurements*. Scientific-Atlanta, Inc, Atlanta Georgia, Jul 1979.

[12] Holzman L. Pillbox Antenna Design for Millimeter Wave Base-station applications. *IEEE Antennas and Propagation Magazine*, Vol.45(1):30–37, Feb 2003.

[13] Hovanessian SA. *Radar System Design and Analysis*. Artech House, Jan 1984.

[14] Inggs M R. SASAR II Design Document. Technical report, University of Cape Town - RRSG, 2003.

[15] Inggs M R. SASAR II Subsystem Requirements. Technical report, University of Cape Town - RRSG, 2003.

[16] Inggs M R. SASAR II User Requirements. Technical report, University of Cape Town - RRSG, 2003.

[17] Jasik H, Johnson R C. *Antenna Engineering Handbook*. McGraw-Hill Book Company, 1961.

[18] Jefferies D. MSc antennas laboratory. http://www.ee.surrey.ac.uk/Personal/D.Jefferies/antmeas.html, Mar 1998.

[19] Kingsley S, Quegan S. *Understanding Radar Systems*. McGraw-Hill Book Company, Jan 1992.

[20] Kraus J D. *Antennas*. McGraw-Hill Book Company, 2nd edition, 1997.

[21] Mohungoo A I. An Airborne SAR Receiver Design and Implementation. Master's thesis, University of Cape Town, 2004.

[22] Orfanidis S J. Electromagnetic Waves and Antennas. The book should be published by the end of 2004, 2004.

[23] Peebles P Z. *Radar Principles*. John Wiley and Sons, 1998.

[24] Pozar D M. *Microwave and RF Design of Wireless Systems*. John Wiley and Sons, 2001.

[25] Rudge A W, Adatia N A. Offset-Parabolic-Reflector Antennas: A Review. In *Proceedings of the IEEE*, volume 66, pages 1592–1618. Institute of Electrical and Electronic Engineers, 1978.

[26] Silver S. *Microwave Antenna Theory and Design*. McGraw-Hill Book Company, 1949.

[27] Skolnik M I. *Radar Handbook, Second Edition*. McGraw-Hill Book Company, Jan 1990.

[28] Stutzman W, Terada T. Design of Offset-Parabolic-Reflector Antennas for Low Cross Pol and Low Sidelobes. *IEEE Antennas and Propagation Magazine*, 35(6):46–49, Dec 1993.